

Dihydro-alkylthio-benzyl-oxypyrimidines as Inhibitors of Reverse Transcriptase: Synthesis and Rationalization of the Biological Data on Both Wild-Type Enzyme and Relevant Clinical Mutants

Claudia Mugnaini,[†] Maddalena Alongi,[†] Andrea Togninelli,[†] Harsukh Gevariya,[†] Antonella Brizzi,[†] Fabrizio Manetti,[†] Cesare Bernardini,[†] Lucilla Angeli,[†] Andrea Tafi,[†] Luca Bellucci,[†] Federico Corelli,[†] Silvio Massa,[†] Giovanni Maga,[‡] Alberta Samuele,[‡] Marcella Facchini,[‡] Imma Clotet-Codina,[§] Mercedes Armand-Ugón,[§] José A. Esté,[§] and Maurizio Botta^{*,†}

Dipartimento Farmaco Chimico Tecnologico, Università degli Studi di Siena, Via Alcide De Gasperi 2, I-53100 Siena, Italy, Istituto di Genetica Molecolare, IGM-CNR, Via Abbiategrasso 207, I-27100 Pavia, Italy, and Retrovirology Laboratori irsiCaixa, Hospital Universitari Germans Trias i Pujol, Universitat Autònoma de Barcelona, E-08916 Badalona, Spain

Received July 9, 2007

A series of novel *S*-DABO analogues, characterized by different substitution patterns at positions 2, 5, and 6 of the heterocyclic ring, were synthesized in a straightforward fashion by means of parallel synthesis and evaluated as inhibitors of human immunodeficiency virus type-1 (HIV-1). Most of the compounds proved to be highly active on the wild-type enzyme both in enzymatic and cellular assays, with one of them emerging as the most active reverse transcriptase inhibitor reported so far ($EC_{50wt} = 25$ pM). The general loss of potency displayed by the compounds toward clinically relevant mutant strains was deeply studied through a molecular modeling approach, leading to the evidence that the dynamic of the entrance in the non-nucleoside binding pocket could represent the basis of the inhibitory activity of the molecules.

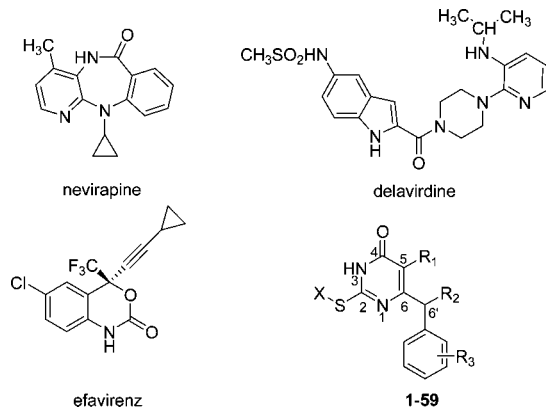
Introduction

Human immunodeficiency virus type-1 (HIV-1^{cr}) infection affects close to 40 million individuals worldwide. Since 1981 when the first case reports of individuals dying from a rare opportunistic infection were published, 20 million people have died from this epidemic. Considerable progress has been made in treating HIV-infected patients in Western countries using highly active antiretroviral therapy (HAART) involving multidrug combinations. However, the spread of many drug-resistant forms of HIV-1 means there is a danger that progress already made will be reversed.¹

The United States Food and Drug Administration (FDA) has to date approved 22 individual agents to directly treat HIV-1 infection. Virus–cell fusion² is blocked by one of these inhibitors, and 10 of these agents target the viral protease, the key enzyme involved in protein maturation and viral assembly. The remainder is directed against the viral reverse transcriptase (RT) and represents the cornerstone of anti-HIV-1 therapies.³

RT is a multifunctional heterodimeric enzyme that converts the genomic HIV RNA into proviral DNA by catalyzing RNA-dependent and DNA-dependent DNA polymerase reactions in addition to RNaseH activities.^{4–6} Drugs targeted at HIV-1 RT

Chart 1. Structure of Known NNRTIs and *S*-DABO Derivatives 1–59



can be divided into two categories: (i) nucleoside and nucleotide analogue RT inhibitors (NRTIs, NtRTIs), which, following activation to their triphosphate forms, compete with RT substrate and also act as terminators of DNA synthesis after incorporation into the primer strand,⁷ and (ii) nonnucleoside RT inhibitors (NNRTIs), including the approved drugs nevirapine, delavirdine, and efavirenz (Chart 1), which, although having wide structural variation, bind at a similar site distal to the active site within RT.^{8–10}

The latter compounds are highly specific for HIV-1 RT and are characterized by less-severe adverse effects than NRTIs. However, the occurrence of just a few single amino acid substitutions in the RT gene can confer resistance to most of the NNRTIs.^{11–16} Therefore, the development of novel NNRTIs with improved pharmacological, pharmacokinetic, and drug resistance mutation profiles is critical for a more successful application of NNRTIs in combination therapy.

Among NNRTIs, dihydro-alkyloxy-benzyl-oxypyrimidines (DABOs) are an interesting class of compounds active at nanomolar concentration.^{17–19} Very recently, we have published

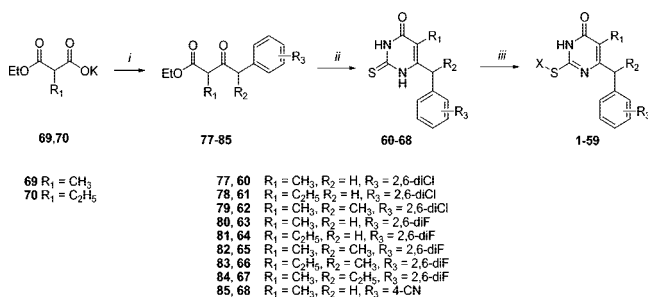
* To whom correspondence should be addressed. Tel.: 0039-(0)577-234306. Fax: 0039-(0)577-234333. E-mail: botta@unisi.it.

[†] Università degli Studi di Siena.

[‡] Istituto di Genetica Molecolare, IGM-CNR.

[§] Universitat Autònoma de Barcelona.

^a Abbreviations: *S*-DABO, dihydro-alkylthio-benzyl-oxypyrimidines; HIV-1, human immunodeficiency virus type-1; RT, reverse transcriptase; EC_{50} , half-maximal effective concentration; HAART, highly active antiretroviral therapy; FDA, Food and Drug Administration; NRTIs, nucleoside reverse transcriptase inhibitors; NtRTIs, nucleotide analogue reverse transcriptase inhibitors; NNRTIs, nonnucleoside reverse transcriptase inhibitors; DABOs, dihydro-alkyloxy-benzyl-oxypyrimidines; AZT, 3'-azidothymidine; TOA, time of addition; RTV, ritonavir; GFA, genetic function approximation; MR, molecular refractivity; LOF, lack of fit; NNBP, non-nucleoside binding pocket; GA-LS, genetic algorithm local search; MD, molecular dynamics.

Scheme 1^a

^a Reagents and conditions: (i) (a) MgCl₂, Et₃N, CH₃CN, rt, 360 rpm, 2 h; (b) substituted phenylacetic acid, *N,N'*-carbonyldiimidazole, rt, 360 rpm, overnight then reflux, 360 rpm, 10 min; (ii) thiourea, EtONa, reflux, 360 rpm, overnight; (iii) substituted benzyl halide, DMF, MW, 130 °C, 5 min (method A); 1-(2-bromoethoxymethyl)-4-methoxybenzene or 4-substituted acetophenone, K₂CO₃, DMF (method B); substituted benzyl alcohol, trimethylphosphine, CBr₄, DMF, MW, 40 °C, 5 min then substituted thioracil, MW, 130 °C, 5 min (Method C); substituted benzyl alcohol, trimethylphosphine, DIAD, DMF, MW, 40 °C, 10 min (method D); substituted aryl boronic acid, Cu(OAc)₂, 1,10-phenantroline, 1,2-DCE, molecular sieves, MW, 85 °C, 10 min (method E).

the synthesis and biological evaluation of a number of *S*-DABO derivatives characterized by the presence of an arylalkylthio substituent of variable length at position 2, a CH₃ group at C-5 and a halogenated benzyl group at the 6 position.^{20–22} Results from anti-HIV-1 RT assays and anti-HIV activity in lymphoid cells showed activity values in the nanomolar and subnanomolar range, respectively. Despite these excellent results on the wild-type (wt) virus strain, lower activity profiles were found when the compounds were tested on mutant strains, thus confirming viral resistance as one of the topical aspects to be explored when designing new NNRTIs.^{13,14,17} As part of a project devoted to structural optimization of the first family of molecules and to the further elucidation of the structure–activity relationships of this class of compounds, we planned to prepare *S*-DABO analogues **1–59** (Chart 1), characterized by different substitution patterns at positions 2, 5, and 6 of the heterocyclic ring. Most of these investigations regarded position 2 where an aryl moiety was connected to the thiopyrimidinone scaffold through spacers of different lengths containing, in some cases, a heteroatom and unsaturated functionalities.

Chemistry

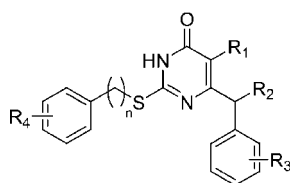
Based on the simple and efficient methodology recently set up in our laboratories,^{21,22} thioracils **60–68** (Scheme 1) were prepared through a parallel solution-phase synthesis using a Büchi Syncore synthesizer. Potassium ethyl 2-substituted malonates **69** and **70** were reacted in parallel with six substituted phenylacetic acids (**71–76**) according to the Clay procedure²³ to give, after simple liquid-phase extractive purification, the β -ketoesters **77–85**. Subsequent condensation of **77–85** with thiourea in the presence of sodium ethoxide afforded the desired thioracils **60–68** in approximately 50% yield. The latter were selectively *S*-benzylated under microwave irradiation with substituted benzyl bromide in dry DMF in the presence of potassium carbonate (method A, compounds **1–7**, **11**, **12**, **14–22**, **25–28**). For compounds **29–32** and **55–59**, the alkylation reaction was performed at room temperature (method B). In the case of **55–59**, this approach was necessary to avoid the formation of compounds deriving from the nucleophilic attack of the S at the benzylic position of the alkylating agent. When the appropriate benzyl bromide was not commercially available, it was prepared from the corresponding alcohol by treatment with carbon tetrabromide and used in situ for the alkylation

reaction (method C, compounds **10**, **13**, **23**, **39**, **41**, **43**, **45–51**, **54**). Alternatively, the *S*-benzylation was carried out using the appropriate benzyl alcohol via a microwave-assisted Mitsunobu reaction in the presence of trimethylphosphine and diisopropyl azodicarboxylate (DIAD) in dry DMF (method D, compounds **8–9**, **24**, **36–38**, **40**, **42**, **44**, **52**, **53**). Compounds having a *p*-methoxy-cinnamic residue directly linked to the sulfur atom were prepared by an Ullman-type reaction using Cu(OAc)₂ and 1,10-phenantroline under microwave irradiation (method E, compounds **33–35**). In all cases, the use of microwaves allowed us to obtain, in a few minutes, the desired products in good yield and high purity (more than 95%, as shown by HPLC-MS analysis).

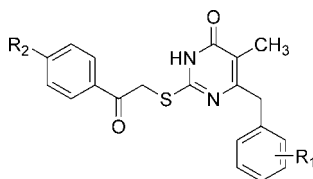
Results and Discussion

The newly synthesized compounds **1–59** were evaluated in enzymatic assays for their ability to inhibit either wt or mutated RTs as well as on MT-4 cells for cytotoxicity and anti-HIV activity, in comparison with AZT, nevirapine, and efavirenz, used as reference drugs. The following mutants were used: K103N and Y181I for enzymatic tests and K103N, Y181C, and Y188L for tests on cell lines. Selected compounds were tested also on IRL98, a clinical isolate, bearing the K101Q, Y181C, and G190A mutations conferring resistance to nevirapine, delavirdine, and efavirenz, respectively. For the sake of clarity, the results of these assays, will be analyzed in separate sections.

Compounds Having a Saturated Alkyl Spacer between S and the Phenyl Ring (1–28, Table 1). As a general consideration, we can say that the substitution pattern on the benzylic moiety at C-6 is fundamental for the biological activity. The substitution at the *para*-position of the benzylic moiety is highly detrimental for the activity, in fact, compounds **25–28**, bearing a 4-CN group on the benzene ring, proved to be completely inactive independently from the substitution at C-2 of the pyrimidinone ring. This result is in agreement with previous findings concerning the corresponding 4-F derivatives.²¹ The 2,6-dichlorobenzyl and 2,6-difluorobenzyl substitutions at C-6 proved conversely to both be highly profitable. In particular, the 2,6-difluorobenzyl group gave the best results when a CH₃ was introduced at the benzylic position. Compounds **20** and **21**, bearing a 4-cyano and a 4-nitrobenzylthio group at C-2, respectively, were endowed with antiviral activity in the low nanomolar range. Among all the compounds tested, compound **19**, characterized by a 4-methoxybenzylthio group at C-2, showed the best activity profile on the wt RT both in enzymatic (ID₅₀ = 3 nM) and in cellular assays (EC₅₀ = 25 pM). On the whole, **19** showed an anti-HIV profile undoubtedly superior to that of nevirapine and comparable to that of efavirenz, thus emerging as the most active RT inhibitor (wt enzyme) reported so far. The EC₅₀ value for compounds **19**, **20**, and **21** proved to be, on wt RT, considerably lower with respect to the corresponding 6-benzyl derivatives.²¹ In particular, the 6-(1-phenylethyl)pyrimidinone **19** is 1000-fold more active than the 6-benzyl counterpart in cellular assays, thus underlying the importance of the 1-(2,6-difluorophenylethyl) moiety for the antiviral activity. Going from a methyl to an ethyl group at the benzylic position, a drop in the activity was observed, with **22** being 2-fold less potent than **19** in cellular assays. In the 2,6-dichloro series, the introduction of a CH₃ group at the benzylic position gave excellent results with **5** and **6**, which showed an EC₅₀ = 1.1 nM and 19 nM, respectively, while in the case of the 4-cyanobenzylthio derivative **7**, a positive effect of the benzyl substitution was observed only in the enzymatic test (ID₅₀ = 20 nM). A positive but more moderate effect was observed

Table 1. Structure and Antiviral Activity of Compounds 1–28

compd	n	R ₁	R ₂	R ₃	R ₄	ID ₅₀ (μM)			EC ₅₀ (μM)				
						wt	K103N	Y181I	NL4-3 wt	K103N	Y181C	Y188L	CC ₅₀
1	1	CH ₃	H	2,6-diCl	4-CH ₃ COO	0.085	>20	>20	0.127	>55.68	8.64	>55.68	>55.68
2	1	C ₂ H ₅	H	2,6-diCl	4-OCH ₃	0.032	7.6	>20	0.0022	6.99	0.83	>57.47	>57.47
3	1	C ₂ H ₅	H	2,6-diCl	4-CN	0.1	>20	>20	0.044	8.84	3.05	>58.14	>58.14
4	1	C ₂ H ₅	H	2,6-diCl	4-NO ₂	0.075	>20	>20	0.0666	>55.55	1.578	>55.55	>55.55
5	1	CH ₃	CH ₃	2,6-diCl	4-OCH ₃	0.77	>20	>20	0.0011	6.72	1.73	42% at 11.49	>11.49
6	1	CH ₃	CH ₃	2,6-diCl	4-NO ₂	0.408	>20	>20	0.019	6.22	7.15	9.95	>11.11
7	1	CH ₃	CH ₃	2,6-diCl	4-CN	0.02	>20	>20	0.16	11.63	39% at 11.63	25% at 11.63	>11.63
8	2	C ₂ H ₅	H	2,6-diCl	4-OCH ₃	0.07	>20	>20	0.0013	6.81	3.85	>11.13	>11.13
9	2	CH ₃	CH ₃	2,6-diCl	4-OCH ₃	0.593	>20	>20	0.0002	6.57	3.76	8.17	>11.13
10	3	CH ₃	CH ₃	2,6-diCl	4-OCH ₃	9.76	>20	>20	0.0002	0.82	0.24	0.28	>10.80
11	1	CH ₃	H	2,6-diF	4-OC ₂ H ₅	0.8	>20	>20	0.37	>62.19	1.19	>62.19	>62.19
12	1	CH ₃	H	2,6-diF	3,4-diOCH ₃	0.5	>20	>20	0.20	9.33	0.74	>39.69	39.69
13	1	CH ₃	H	2,6-diF	3,4-OCH ₂ O	>20	>20	>20	0.15	10.22	1.32	>62.19	44% at 62.19
14	1	CH ₃	H	2,6-diF	4-CH ₃ COO	48	>20	>20	22.88	>60.10	>60.10	>60.10	>60.10
15	1	CH ₃	H	2,6-diF	4-CH ₃ OCO	0.5	>20	>20	0.142	11.18	1.35	>34.09	>34.09
16	1	C ₂ H ₅	H	2,6-diF	4-OCH ₃	0.03	>20	>20	0.012	10.30	1.45	>62.19	>62.19
17	1	C ₂ H ₅	H	2,6-diF	4-CN	0.17	7.5	>20	0.075	7.78	1.33	>62.97	>62.97
18	1	C ₂ H ₅	H	2,6-diF	4-NO ₂	0.07	>20	>20	0.074	10.6	2.13	>59.95	>59.95
19	1	CH ₃	CH ₃	2,6-diF	4-OCH ₃	0.003	45	>20	0.000025	0.55	0.30	0.95	>12.43
20	1	CH ₃	CH ₃	2,6-diF	4-CN	0.01	0.7	>20	0.0078	0.73	1.55	0.68	>12.59
21	1	CH ₃	CH ₃	2,6-diF	4-NO ₂	0.03	0.6	>20	0.0033	0.66	0.44	0.22	>11.99
22	1	CH ₃	C ₂ H ₅	2,6-diF	4-OCH ₃	0.047	>20	>20	0.0019	6.13	5.02	1.46	>12.02
23	2	CH ₃	H	2,6-diF	4-OCH ₃	0.029	3.5	>20	0.0049	4.13	6.34	8.53	>62.19
24	2	C ₂ H ₅	H	2,6-diF	4-OCH ₃	0.022	>20	>20	0.0002	1.923	2.78	>60.10	>60.10
25	1	CH ₃	H	4-CN	4-OCH ₃	>20	>20	>20	20.32	>66.31	>66.31	>66.31	>66.31
26	1	CH ₃	H	4-CN	4-C ₄ H ₉	>20	>20	>20	4.57	>79.87	>79.87	>79.87	>79.87
27	1	CH ₃	H	4-CN	4-NO ₂	>20	>20	>20	>26.43	>26.43	>26.43	>26.43	26.43
28	1	CH ₃	H	4-CN	4-CN	>20	>20	>20	>67.20	>67.20	>67.20	>67.20	>67.20

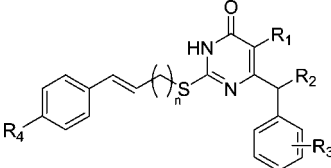
Table 2. Structure and Antiviral Activity of Compounds 29–32

compd	R ₁	R ₂	ID ₅₀ (μM)			EC ₅₀ (μM)				
			wt	K103N	Y181I	NL4-3 wt	K103N	Y181C	Y188L	CC ₅₀
29	2,6-diCl	CN	0.2	>20	>20	1.08	12.21	1.31	>56.31	>56.31
30	2,6-diF	NO ₂	0.95	>20	>20	0.37	>58.00	4.18	>58.00	>58.00
31	2,6-diF	Cl	7.5	>20	>20	3.76	>59.52	3.69	>59.52	>59.52
32	4-CN	H	>20	>20	>20	>67.20	>67.20	>67.20	>67.20	>67.20

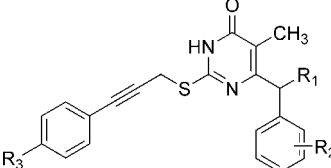
with the introduction of an ethyl group at C-5. EC₅₀ values resulted in the nanomolar range for compounds **16–18**, with the best profile shown by the 4-methoxybenzylthio derivative **16** both in enzymatic and cellular assays. The corresponding 2,6-dichlorobenzyl derivatives **2–4** exhibited a similar behavior, confirming the 4-methoxybenzylthio substitution at C-2 as the most profitable (**2**, ID₅₀ = 32 nM, EC₅₀ = 2.2 nM). On the other hand, very potent compounds were obtained, increasing the length of the linker connecting the S atom to the phenyl ring. Among them, **8**, **9**, **23**, and **24** (*n* = 2) proved to be the most potent inhibitors, with an EC₅₀ value ranging from 0.2 nM to 4.9 nM in cellular tests. In particular, the introduction of an ethyl group at C-5 (compound **24**) and a methyl group at the benzylic position (compound **9**) proved to be the most

effective modifications. Comparable results (EC₅₀ = 0.2 nM) were obtained with **10**, characterized by a three-carbon spacer and a methyl group at the benzylic position. Conversely, when a higher alkoxy group was introduced on the benzene ring, maintaining a one-carbon spacer (compound **11**), the positive effect of the chain lengthening was lost, giving raise to an almost inactive compound.

Compounds Having a Phenacyl Moiety Linked to the Sulfur Atom (29–32, Table 2). The introduction of a 4-substituted phenacylthio group at C-2 resulted in a significant reduction of the activity, with compounds **29–31** displaying activities in the micromolar range and **32** being completely inactive.

Table 3. Structure and Antiviral Activity of Compounds 33–51


compd	n	R ₁	R ₂	R ₃	R ₄	ID ₅₀ (μM)			EC ₅₀ (μM)				CC ₅₀
						wt	K103N	Y181I	NL4-3 wt	K103N	Y181C	Y188L	
33	0	CH ₃	H	2,6-diCl	F	>20	>20	>20	>59.38	11.88	>59.38	>59.38	>59.38
34	0	CH ₃	H	2,6-diCl	OCH ₃	1.98	>20	>20	>57.74	>57.74	>57.74	>57.74	>57.74
35	0	CH ₃	CH ₃	2,6-diCl	OCH ₃	0.02	>20	>20	16.22	>55.93	>55.93	>55.93	>55.93
36	1	CH ₃	H	2,6-diCl	OCH ₃	0.007	9.0	>20	0.015	>0.96	>0.96	>0.96	0.96
37	1	CH ₃	H	2,6-diCl	NO ₂	3.81	>20	>20	>10.82	>10.82	>10.82	>10.82	>10.82
38	1	CH ₃	H	2,6-diCl	N(CH ₃) ₂	0.778	>20	>20	>54.35	>54.35	>54.35	>54.35	>54.35
39	1	C ₂ H ₅	H	2,6-diCl	CN	0.188	>20	>20	1.73	>54.82	41% at 54.82	>54.82	>54.82
40	1	C ₂ H ₅	H	2,6-diCl	OCH ₃	0.056	>20	>20	0.0015	>0.19	>0.19	>0.19	0.19
41	1	C ₂ H ₅	H	2,6-diCl	NO ₂	2.5	>20	>20	0.61	>32.14	4.2	>32.14	32.14
42	1	CH ₃	CH ₃	2,6-diCl	OCH ₃	0.018	>20	>20	0.009	2.47	3.6	1.26	>10.84
43	1	CH ₃	CH ₃	2,6-diCl	NO ₂	0.102	>20	>20	0.48	>40.97	>40.97	>40.97	40.97
44	1	CH ₃	H	2,6-diF	NO ₂	11.88	>20	>20	0.26	>11.65	>11.65	>11.65	11.65
45	1	CH ₃	H	2,6-diF	OCH ₃	0.25	>20	>20	0.043	>3.93	>3.93	>3.93	3.93
46	1	CH ₃	CH ₃	2,6-diF	NO ₂	0.283	>20	>20	0.14	>11.28	>11.28	>11.28	>11.28
47	1	CH ₃	CH ₃	2,6-diF	OCH ₃	0.292	3.7	>20	0.0002	0.26	0.13	0.07	>11.7
48	1	CH ₃	CH ₃	2,6-diF	CN	0.161	>20	>20	0.14	>59.1	>59.1	>59.1	>59.1
49	1	C ₂ H ₅	CH ₃	2,6-diF	OCH ₃	0.016	0.4	>20	0.0002	1.02	0.70	0.63	5.54
50	1	C ₂ H ₅	CH ₃	2,6-diF	NO ₂	0.009	>20	>20	0.0004	>5.75	>5.75	1.94	5.75
51	1	C ₂ H ₅	CH ₃	2,6-diF	CN	0.048	>20	>20	0.59	>27.23	>27.23	>27.23	27.23

Table 4. Structure and Antiviral Activity of Compounds 52–54


compd	R ₁	R ₂	R ₃	ID ₅₀ (μM)			EC ₅₀ (μM)				CC ₅₀
				wt	K103N	Y181I	NL4-3 wt	K103N	Y181C	Y188L	
52	H	2,6-diCl	OCH ₃	0.01	>20	>20	2.47	>56.18	40% at 56.18	>56.18	>56.18
53	CH ₃	2,6-diCl	OCH ₃	0.005	>20	>20	0.50	>54.47	33.55	24.84	>54.47
54	H	2,6-diF	NO ₂	0.416	>20	>20	40.09	>58.55	>58.55	>58.55	>58.55

Compounds Having an Unsaturated Alkyl Spacer between S and the Phenyl Ring (33–54, Table 3, Table 4).

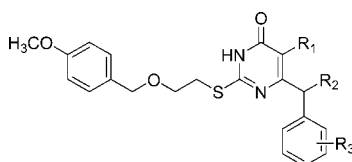
The introduction of a cinnamic functionality proved to be particularly profitable for the compounds characterized by 2,6-difluorobenzyl substitution at C6. Excellent results were obtained for compounds 47, 49, and 50, having a methyl group at the 6' position with an activity in cellular tests in the subnanomolar range. In the 2,6-dichlorobenzyl series, compound 40, characterized by the presence of an ethyl instead of a methyl group at C-5, showed an activity in the low nanomolar range. On the other hand, the substitution of the double bond with a triple bond led to less-active compounds in both the 2,6-difluorobenzyl and the 2,6-dichlorobenzyl series.

Compounds Having a *p*-Methoxybenzyloxyethyl Group Linked to S (55–59, Table 5). The introduction of a *p*-methoxybenzyloxyethylthio group at position 2 of the pyrimidinone scaffold had, in most cases, a positive effect on the activity both at the enzymatic level and at the cellular level. In particular, compound 58, having a CH₃ at the 6'-position and belonging to the difluoro series, showed the best profile, with an ID₅₀ = 8.3 nM and an EC₅₀ = 1.1 nM. Its activity on the

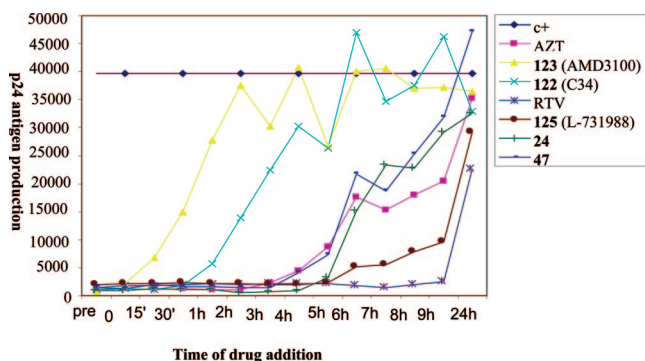
mutant strains was, at the cellular level, in the submicromolar range, with a medium fold resistance value of 500. Interesting results were also obtained in the dichloro series, with compounds 55 and 56 having an antiviral activity in the medium nanomolar range.

As a result of the emergence of some contradictions from the analysis of the biological data between ID₅₀ and EC₅₀ values, time-of-addition (TOA) experiments were performed on two selected molecules (24 and 47) to investigate the possibility of a different mechanism of action at the molecular level for these compounds (Figure 1). Chart 2 shows compounds 122, 123, AZT, 124, and ritonavir (RTV) used as reference compounds for fusion, entry, RT, integrase, and protease inhibitors, respectively. Because both 24 and 47 showed, in TOA experiments, a behavior more similar to that of AZT (the RTI control) than to that of the control integrase inhibitor 124, it was concluded that they act as reverse transcriptase inhibitors. These results are in line with their resistance profile, which suggests they work as NNRTIs.

Taking into account the results obtained when the newly synthesized compounds were tested against a panel of mutant strains of the virus, some interesting considerations emerge.

Table 5. Structure and Antiviral Activity of Compounds 55–59

compd	R ₁	R ₂	R ₃	wt	ID ₅₀ (μM)			EC ₅₀ (μM)			
					K103N	Y181I	NL4-3 wt	K103N	Y181C	Y188L	CC ₅₀
55	CH ₃	H	2,6-diCl	0.063	56.01	>20	0.021	3.44	3.01	1.72	>53.76
56	CH ₃	CH ₃	2,6-diCl	0.022	57.31	>20	0.063	6.47	8.98	2.5	39.04
57	CH ₃	H	2,6-diF	0.197	>20	>20	1.20	>55.87	>55.87	>55.87	>55.87
58	CH ₃	CH ₃	2,6-diF	0.0082	9.94	>20	0.0011	0.92	0.65	0.32	30.72
59	C ₂ H ₅	CH ₃	2,6-diF	0.741	>20	0.27	3.89	>54.35	>54.35	>54.35	>54.35

**Figure 1.** Time of drug addition experiments.

While most of the compounds showed fold of resistance values too high to be further investigated, a number of them exhibited values comparable to those of commercial drugs, such as nevirapine and efavirenz, with an EC₅₀ value in the high nanomolar range against most of the mutants studied. For these compounds, the activity against mutant IRL98 was also evaluated (Table 6). Interestingly, among them, **3**, **17**, **20**, and **29** share a common feature, that is, the presence of the 4-cyanobenzylthio moiety at C-2, which could represent a starting point for the development of new molecules potentially endowed with potent activity on the most relevant mutant strains. Moreover, we can also say that the newly synthesized compounds show a general resistance profile that is definitely better with respect to the compounds of the first series,²¹ thus underlying the importance of the right combination of substituents at C-2 and C-6 responsible for the activity on mutant K103N and Y181C/Y188L, respectively.

Molecular Modeling Calculations

1. Rationalization of the Biological Data on wt RT through a QSAR Approach. The new compounds, together with additional *S*-DABOs, previously described by us (**86–121**, Table 7),^{20,21} were submitted to a 3D QSAR analysis with the aim of identifying molecular determinants able to influence their activity.

For this purpose, the Genetic Function Approximation (GFA) algorithm of the QSAR+ module, implemented in Cerius2,²⁴ was applied. In particular, 95 compounds, with activity data spanning over 6 orders of magnitude (from 0.025 to 67000 nM) were divided into a training set (52 compounds) and a test set (43 compounds).

In general, it is important to note that the building of a statistical model able to correlate the activity of *S*-DABOs with their structural properties was a very difficult task. In fact,

attempts to generate QSAR models based on both 2D and 3D descriptors led to no significant results, suggesting that 3D information in our hands (derived from docking calculations) was useless to QSAR purposes. Similarly, the application of QSAR techniques to enzymatic data was unsuccessful in obtaining equations able to correlate structure and activity of compounds. Finally, the sole cellular data (as independent variable) and several 2D descriptors (as dependent variables) gave a set of statistically significant equations, mainly based on topological descriptors.

The best scored equations derived from GFA calculations on training set compounds (Table 8) shared very similar information content, in terms of type of descriptors. In fact, they were characterized by the frequent presence of topological descriptors, such as Kier-Hall subgraph count indices (SC-X_n), electrotopological descriptors (such as S_sF),²⁵ and molecular refractivity (MR). A brief description of molecular descriptors found in QSAR equations is reported in Table 9.

Equations were also characterized by different levels of complexity, and their predictive power was assessed by both internal and external validation procedures. Equation 1, with a satisfactory *r*² (0.60) and the lowest LOF value, as well as with the best cross-validated correlation coefficient *q*² (0.50), was chosen as the election equation. Internal validation of the model showed that estimated activity values for most of the compounds of the training set were largely within 1 log unit, with only three compounds whose activities were completely mispredicted by the model (errors higher than 2 log units; Figure 2, Table 10). On the other hand, the external validation of eq 1 toward the test set led to a poor *r*² (0.28). Although most of the activity values were predicted with errors lower than 1 order of magnitude, three exceptions (compounds **121**, **12**, and **38**) showed marked prediction errors (about 12, 2.2, and 2.4 log units, respectively), strongly suggesting that the model was unable to handle such compounds. Inspection of the molecular structure of **121** revealed that it is the sole compound bearing an anthraquinone moiety at R₁. As a consequence, it is likely that the model itself has not been trained to handle this kind of group, resulting in a high error of prediction. For this reason, **121** was classified as an outlier and removed from the test set, allowing *r*² to rise up to 0.56.

GFA calculations showed that cellular activity of *S*-DABOs mainly depended on the subgraph count indices that measure the degree of structural complexity of a molecule, describing the number of third- and fifth-order subgraphs in the molecular graph (i.e., the number of paths of length 3 and 5, respectively). In detail, while SC-3_P resulted to be directly correlated to the cell inhibitory activity (positive sign), SC-5_P badly affected it (negative sign). This result could indicate that long paths (such

Chart 2

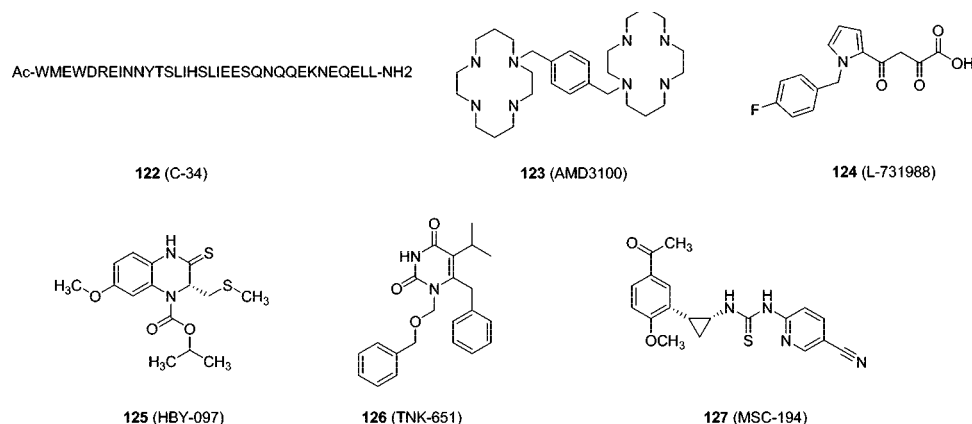


Table 6. Fold Resistance Values of Selected Compounds against a Panel of Mutant Strains In Comparison to Those of AZT, Nevirapine, and Efavirenz

cmpd	EC ₅₀ (μM) toward NL4-3wt	fold resistance			
		IRLL98	K103N	Y181C	Y188L
3	0.044	194	200	69	>1321
12	0.20	1.5	46	3.7	>198
13	0.15	1.8	68	8.8	>415
15	0.142	6.9	78	9.5	>240
17	0.075	45.3	104	18	>840
20	0.0078		93	199	87
29	1.08	3.2	11.3	1.2	>51
AZT	0.003	3	1		1
NVP	0.052	144	70		144
EVZ	0.001	300	80		400

as paths of length higher than 5) were not profitable for activity, while shorter paths (such as order 3) were favored. Moreover, a comparison between eqs 1 and 5 suggested that both MR and S_sF (an electrotopological descriptor accounting for the presence of fluorine atoms into the inhibitor structure) parameters play a significant role in accounting for activity data (in fact, such descriptors represent the major differences between the two equations that share the remaining three terms). This result is in good agreement with the fact that many of the most active compounds have one or two fluorine substituents on their structure, such as **19** (the most active compound). Moreover, the presence of MR (measuring the volume and density of the compounds) and its positive coefficient seemed to show that the binding site for these compounds has a certain tolerance to the bulkiness of the inhibitors. In agreement with this hypothesis, compounds bearing a methyl substituent at C6' showed an activity in principle higher than that of the corresponding unsubstituted analogues.

2. Rationalization of the Biological Data on K103N, Y181C, and Y188L through Molecular Docking and Molecular Dynamics Simulations. Following our previous efforts aimed at studying the binding mode of *S*-DABOs into the non-nucleoside binding pocket (NNBP) of wt RT²¹ and with the idea to rationalize the general loss of potency of the compounds on the mutated enzyme, molecular docking simulations were performed by means of the software Autodock 3.0 using the structure of three different mutants of RT.²⁶ The X-ray crystallographic structure of the complexes between RT and **125** (Y188L mutant, PDB entry 1BQN),²⁷ **126** (mutant Y181C, PDB entry 1JLA),²⁸ and **127** (K103N mutant, PDB entry 1IKY)²⁹ were used for docking calculations (Chart 2).

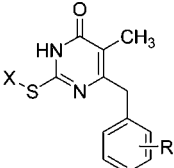
In a preliminary step, the reliability of the docking protocol was tested by simulations of the binding mode of RT inhibitors

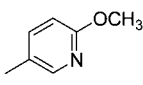
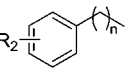
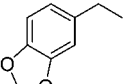
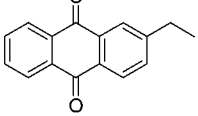
125 and **126** and by a comparison of the modeled complexes with the available 3D structures derived by X-ray crystallography (1BQN and 1JLA, respectively). Structures of inhibitors were built using Maestro 3D-sketcher,³⁷ minimized with OPLS_AA force field³⁸ using the Polak-Ribiere conjugated gradient method (0.01 kJ/Å³•mol convergence) and finally docked in the native protein. The experimental binding conformations of the reference compounds were successfully reproduced applying the default settings of the GA-LS method with 250 docking runs. In particular, the first ranked docked conformation belonging to the most populated cluster (239 conformers) was able to reproduce the X-ray conformation of **126** with a root-mean-square deviation (rmsd) of 0.71 Å calculated on all of atom coordinates. On the other hand, the best conformation of **125** belonging to the most populated cluster (39 conformers) reproduced the crystallographic pose with a 1.88 Å rmsd calculated on all of atom coordinates. Moreover, a comparison between calculated and experimental affinity showed that HBY-097 had an estimated value of 0.4 μM versus an experimental value of 0.6 μM (affinity of **126** toward Y181C RT is not available).

With a reliable docking procedure in our hands, in the next step of the computational work we used the crystallographic structure of the RT mutants to dock the *S*-DABO compounds.

Although structures of several drug-resistant RT mutants in complex with inhibitors are available, the complex network of factors contributing to resistance is not completely understood yet. It is known that the most obvious result of drug-resistant mutations, such as the frequent Y181C and Y188L substitutions, is the loss of contacts between the bound inhibitor and the substituted amino acid. However, other mutated amino acids associated with resistance do not interact directly with inhibitors, indicating that different mechanisms of action could also occur. For example, K103N substitution, that is one of the most frequently observed upon therapeutic interventions involving NNRTIs, is located at the outer rim of the pocket where NNRTIs bind and is very seldom involved in direct interactions with the bound drugs, as found in a number of crystallographic complexes.³⁰

Shen et al. have recently shown that NNBP possess a very flexible structure, allowing RT to accommodate inhibitors characterized by different structural shapes and sizes.³¹ In their paper, the authors present the results of long-lasting molecular dynamics (MD) runs, simulating the unbinding process of a non-nucleoside inhibitor (α-APA) from HIV-1 RT. The unbinding process has been condensed into three phases based on the position of the ligand with respect to the binding pocket: phase

Table 7. Structure of Compounds **86–121** Already Reported by us and Used in this Work for Computational Aims


86: X = 
87-119: X = 
120: X = 
121: X = 

cmpd	R ₁	R ₂	n
86	2,6-diCl		
87	2,6-diCl	4-F	0
88	2,6-diCl	4-OCH ₃	0
89	2,6-diCl	H	0
90	2,6-diF	H	0
91	2,6-diF	4-F	0
92	2,6-diF	4-OCH ₃	0
93	2,6-diCl	4-CN	0
94	2,6-diCl	4-OCH ₃	1
95	2,6-diCl	H	1
96	2,6-diCl	4-NO ₂	1
97	2,6-diCl	4-F	1
98	2,6-diCl	3-Cl	1
99	2,6-diCl	3-F	1
100	4-F	4-OCH ₃	1
101	2,6-diF	4-OCH ₃	1
102	2,6-diF	4-NO ₂	1
103	2,6-diCl	3-CN	1
104	2,6-diF	4-CN	1
105	2,6-diCl	4-OH	1
106	2,6-diCl	4-Br	1
107	2,6-diCl	3,4-diOCH ₃	1
108	2,6-diCl	4-CH ₃ CH ₂ O	1
109	2,6-diCl	4-OCH ₃	2
110	2,6-diF	2,3-diOCH ₃	1
111	2,6-diCl	4- <i>i</i> Pr	1
112	2,6-diCl	2,3-diOCH ₃	1
113	2,6-diF	4- <i>i</i> Pr	1
114	2,6-diCl	4-Cl	1
115	4-F	4-NO ₂	1
116	2,6-diCl	4-CN	1
117	2,6-diCl	2,4-diOCH ₃	1
118	2,6-diCl	4-CH ₃ CH ₂ CH ₂ CH ₂ O	1
119	2,6-diCl	4-OCH ₃	3
120	2,6-diCl		
121	2,6-diCl		

I, associated with the escape from the binding pocket toward the putative entrance of it; phase II, in which the ligand “overcomes steric conflicts” with the residues at the entrance and exits from the binding pocket; and phase III, during which the ligand moves away from protein surface and enters the solvent. According to the authors, phase II represents the bottleneck of the entire binding/unbinding process. On the other hand, Rodriguez-Barrios et al. have simulated the opening of the NNBP entrance in the presence of K103N mutation.³⁰ By their studies, these authors explain drug resistance of the mutant enzyme, as due to “the existence of a higher energy barrier to pocket creation in this mutant enzyme with respect to wild-type”. Therefore, it is reasonable to assume that the understanding of the resistance profile of NNRTIs is unlikely to be gained

just by docking studies, whereas we must admit that a relationship should exist, at least in the case of the K103N mutation, between the activity of a compound and its faculty to create the pocket in the entrance zone of the binding pocket. That is to say that the whole process, consisting of the formation of the allosteric site and of its occupation, must sometimes be investigated.

Docking Simulations on the Y188L Mutant. To better analyze the relationships between the structures of compounds **1–59** and their activity toward Y188L RT, compounds were divided into two classes: unsubstituted compounds at position 6′ (**1–4**, **8**, **11–18**, **23–34**, **36–41**, **44**, **45**, **52**, **54**, **55**, and **57**) and 6′-methyl- or 6′-ethyl-substituted compounds (**5–7**, **9**, **10**, **19–22**, **35**, **42**, **43**, **46–51**, **53**, **56**, **58**, and **59**).

Among 6′-methyl derivatives bearing at position 2 of the pyrimidinone nucleus a saturated alkyl spacer between the sulfur atom and the phenyl ring (**1–28**), compounds **10**, **19**, **20**, **21**, and **22** were found to be the most active inhibitors. Docking simulations showed that they share a common binding mode into the NNBP. As an example, the *R*-enantiomer of compound **19** assumed an orientation very similar to that of the cocrystallized inhibitor **125**, a quinoxaline derivative (Figure 3). In particular, the pyrimidinone ring was superposable to the heterocyclic portion of the quinoxaline ring of **125** and was involved in two hydrogen bond contacts between its NH (corresponding to N2 of **125**) and CO groups (corresponding to S1 of **125**) with the CO and NH moieties of Lys101 backbone (1.8 Å and 2.0 Å distance, respectively), suggested to be crucial interaction keys for inhibitors belonging to the DABO and *S*-DABO classes of compounds.¹⁸

The extended side chain at position 2 of **19** was partially superimposed to the aromatic moiety of the quinoxaline ring of **125** and pointed toward residues (namely, Pro225, Phe227, and Pro236) of the solvent-accessible surface. In further detail, the sulfur atom of the inhibitor was located at a distance of about 4.8 Å from the backbone NH group of Lys101, and the *p*-methoxybenzyl moiety was accommodated into a large pocket mainly defined by Val106, Pro225, Pro236, and Phe227. Good profitable hydrophobic interactions were found between the alkyl side chain of Val106 and the phenyl ring of the C2 side chain of the inhibitor, as well as between the terminal methyl group (of the methoxy substituent) with both Pro225 and Pro236. The methyl group at C5 of the pyrimidinone ring, located in the same region accommodating the methylthiomethylene group of the cocrystallized inhibitor, was located in a hydrophobic pocket delimited by Val179, Leu188, and Gly190. The benzyl substituent at C6, superimposable to the isopropoxycarbonyl group of **125**, was embedded into an extended hydrophobic region defined by the aromatic side chains of Tyr181, Phe227, and Trp229, as well as by Leu100 and Leu234. Finally, for both the enantiomers of **19**, hydrophobic interactions were also found between the methyl group at position 6′ and the side chain of Leu188 (distances between the methyl group of *R*- and *S*-enantiomers from the methyl of Leu188 were 3.74 and 3.71 Å, respectively).

Computational results showed that the binding mode of all the docked compounds were similar in complexes with both the wt and Y188L RT, suggesting that no significant differences occurred in the interactions between the inhibitors and the two forms of the enzyme, with the exception of the contacts involving the amino acid residue 188. In fact, loss of drug-enzyme interactions at the level of Tyr188 could account for the generally reduced potency of compounds toward the Y188L mutant, in comparison to the wt RT. In fact, the aromatic side

Table 8. QSAR Results: Details of the Best 10 Generated Equations^a

equation	LOF	r^2	q^2	r^2_{test}	variables
$\text{pIC}_{50} = 0.313408 + 0.086705 * \text{"MR"} + 2.33291 * \text{"SC-3_P"} - 0.128763 * \text{"E-ADJ-mag"} - 0.7349 * \text{"SC-5_P"} + 0.059466 * \text{"S_sF"}$	2.21	0.60	0.50	0.56	5
$\text{pIC}_{50} = 14.6538 + 2.17464 * \text{"SC-3_P"} - 0.803465 * \text{"SC-5_P"} + 0.051067 * \text{"S_sF"} + 0.082478 * \text{"MR"} - 0.477012 * \text{"Zagreb"}$	2.39	0.57	0.47	0.22	5
$\text{pIC}_{50} = 15.1165 - 0.345684 * \text{"SC-4_PC"} - 0.983279 * \text{"SC-5_P"} + 0.064886 * \text{"S_sF"} + 0.097409 * \text{"MR"} - 0.669639 * \text{"Zagreb"} + 3.1391 * \text{"SC-3_P"}$	2.41	0.62	0.50	0.20	6
$\text{pIC}_{50} = 18.085 + 0.180462 * \text{"IAC-Total"} - 0.705413 * \text{"SC-5_P"} - 0.564866 * \text{"Zagreb"} + 2.07671 * \text{"SC-3_P"}$	2.46	0.50	0.39	0.17	4
$\text{pIC}_{50} = 0.322936 - 0.657856 * \text{"SC-5_P"} + 2.14235 * \text{"SC-3_P"} - 0.104946 * \text{"E-ADJ-mag"}$	2.46	0.43	0.32	0.24	3
$\text{pIC}_{50} = -3.26636 + 2.42884 * \text{"SC-3_P"} - 0.108766 * \text{"E-ADJ-mag"} - 0.82768 * \text{"SC-5_P"} + 0.058926 * \text{"S_sF"} + 0.089015 * \text{"MR"} - 0.000681 * \text{"V-DIST-mag"}$	2.47	0.62	0.48	0.52	6
$\text{pIC}_{50} = 13.2513 + 2.10752 * \text{"SC-3_P"} - 0.748813 * \text{"SC-5_P"} - 0.415727 * \text{"Zagreb"}$	2.48	0.42	0.33	0.16	3
$\text{pIC}_{50} = 1.95177 + 2.13197 * \text{"SC-3_P"} - 0.107145 * \text{"E-ADJ-mag"} - 0.654289 * \text{"SC-5_P"} - 0.117996 * \text{"S_tN"}$	2.50	0.49	0.38	0.24	6
$\text{pIC}_{50} = -2.24815 + 2.39023 * \text{"SC-3_P"} - 0.111983 * \text{"E-ADJ-mag"} - 0.822868 * \text{"SC-5_P"} + 0.057953 * \text{"S_sF"} + 0.086431 * \text{"MR"} - 0.001042 * \text{"Wiener"}$	2.50	0.61	0.47	0.53	6
$\text{pIC}_{50} = -2.86735 - 0.000527 * \text{"E-DIST-mag"} + 2.39235 * \text{"SC-3_P"} - 0.112218 * \text{"E-ADJ-mag"} - 0.787158 * \text{"SC-5_P"} + 0.057686 * \text{"S_sF"} + 0.086125 * \text{"MR"}$	2.51	0.61	0.47	0.53	6

^a The q^2 values were calculated excluding compound **121**, which was considered as an outlier. LOF, r^2 , q^2 , and r^2_{test} are the lack-of-fit, the correlation coefficient, the cross-validated correlation coefficient, and the correlation coefficient calculated on the test set, respectively. A brief description of molecular descriptors is reported in Table 9.

Table 9. Summary of the 12 Molecular Descriptors Contributing to the QSAR Models

no.	descriptor ^a	type	description
1	MR	thermodynamic	molar refractivity
2	SC-3_P	topological	number of third-order subgraph in the molecular graph: the number of paths of length 3
3	SC-4_PC	topological	number of third-order subgraph in the molecular graph: the number of paths of length 4
4	SC-5_P	topological	number of third-order subgraph in the molecular graph: the number of paths of length 5
5	Zagreb	topological	sum of the squares of vertex valencies
6	Wiener	topological	sum of lengths of minimal paths between all pairs of vertices representing the heavy atoms
7	S_sF	electrotopological	fluoride with 1 single bond
8	S_tN	electrotopological	N with 1 triple bond
9	E-ADJ-mag	information content	edge adjacency/magnitude
10	IAC-Total	information content	entropy of elements distribution
11	V-DIST mag	information content	variety of vertex distance matrix
12	E-DIST-mag	information content	edge distance/magnitude

^a Further details on molecular descriptors are available at the QSAR+ theory page of the Accelrys Web site http://www.accelrys.com/doc/life/cerius481/qsar/Output/theory_d_nf.html.

chain of wt Tyr188 showed extensive van der Waals interactions with the C6 benzyl moiety of inhibitors. These hydrophobic interactions were in principle lost in the complexes with the mutated RT, although compounds **10**, **19–22** partially restored them as contacts between their 6'-methyl or 6'-ethyl substituent, which interacted with the Leu188 side chain. In confirmation of the importance of these hydrophobic contacts, the unsubstituted inhibitors **2**, **16**, **101**, **102**, **104**, and **119**, which did not interact with Leu188, were found to be inactive toward the mutant.

Moreover, compounds **29–32**, bearing a phenacyl moiety linked to the sulfur atom but devoid of substituents at position 6', were unable to interact with the Leu188 side chain and, accordingly, were inactive toward Y188L RT.

Among compounds **33–51**, bearing a cinnamyl moiety at position 2, derivatives **42**, **47**, **49**, and **50**, although less-active toward the mutated enzyme than toward the wt, maintained some activity, probably because of the presence of a 6'-methyl group. Noteworthy, compound **47** showed the best activity toward Y188L RT ($\text{EC}_{50} = 70 \text{ nM}$, fold resistance toward wt = 35,

$\text{K103N} = 3.7$, and $\text{Y181C} = 1.9$). Finally, activity of compounds **55–59**, having a *p*-methoxybenzyloxyethyl group linked to S, was more difficult to explain. In fact, **55** was active although it was unsubstituted at position 6', while **59** was inactive although bearing a methyl group at the same position.

The binding mode of compounds **19** ($\text{EC}_{50\text{Y188L}} = 0.95 \mu\text{M}$) and the corresponding 6'-unsubstituted **101** ($\text{EC}_{50\text{Y188L}} = 10 \mu\text{M}$) is represented in Figure 4 as an example of the importance of the additional interaction of the 6'-CH₃ with the Leu188 side chain.

Docking Simulations on the Y181C Mutant. Also in this case, in an attempt to make SAR considerations, compounds **1–59** were divided into classes on the basis of the presence of a methyl (**1**, **5–7**, **9–15**, **19–23**, **25–38**, **42–48**, **52–58**) or ethyl group (**2–4**, **8**, **16–18**, **24**, **39–41**, **49–51**, **59**) at position 5 of the pyrimidinone ring.

The binding mode of **16** into NNBP of Y181C RT was similar to that found for **19** into NNBP of Y188L RT. In particular, the NH group of **16** interacted by a hydrogen bond with the carbonyl moiety of Lys101 (1.75 Å distance), as well as the

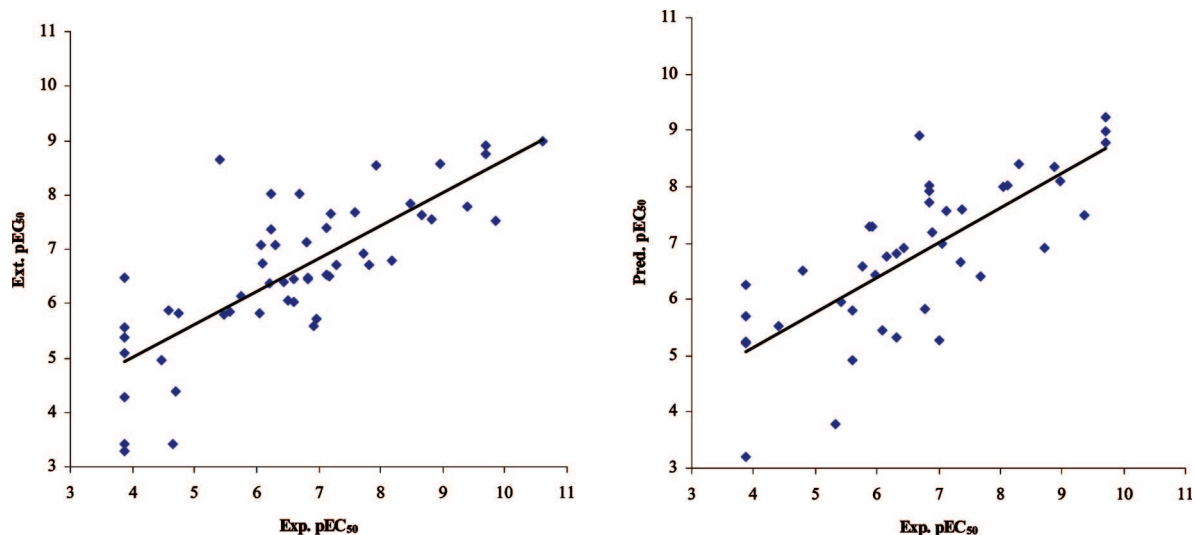


Figure 2. Scatter plots for training (left) and test sets (right).

fluorine atom of the inhibitor and the sulfur of Cys181 were potentially hydrogen bonded. The benzyl group at position 6 is embedded into an aromatic cage formed by Tyr188, Phe227, and Trp229 and showed profitable hydrophobic interactions also with Leu100 and Leu234. However, the hydrophobic contact of the ethyl substituent at position 5 with the side chain of Cys181 appeared to be the most important interaction between the inhibitor and RT. Shortening of such an ethyl group to a methyl substituent (as in **101**, previously reported)²¹ led to a compound inactive toward Y181C RT (data not shown), probably because the lack of the contact involving Cys181 side chain. In a similar way, among compounds **1–28**, bearing a 2-benzylthio substituent, derivatives with an ethyl group at position 5 (**2–4**, **8**, **16–18**, and **24**) were active against Y181C, while the methylated compounds (**94**, **96**, **101**, **102**, **104**, and **109**) were inactive (data not shown). On the other hand, compounds with a methyl or ethyl group at position 6' (**5–7**, **9**, **10**, **19–22**) retained some activity toward Y181C RT, independently from the presence of a methyl or ethyl group at position 5, confirming the important role played by the introduction of a small lipophilic substituent at the 6'-benzylic position.

Activity data of compounds with a cinnamyl moiety at position 2 (**33–51**) followed the same trend found for **1–28**. However, while the last compounds showed an activity independent from the substituent on the extended side chain at position 2 (4-methoxybenzylthio, 4-nitrobenzylthio, and 4-cyanobenzylthio moieties), the *p*-methoxy group of **33–51** seemed to be the most convenient substituent. In fact, **47** and **49**, both bearing a *p*-methoxy cinnamyl at position 2, a methyl at position 6', and a 5-methyl or 5-ethyl group, respectively, were the most potent inhibitors of the series. In this context, it is important to note that, because the binding mode and the interactions of compounds with a 4-methoxy (**40** and **49**), a 4-nitro (**41** and **50**) and a 4-cyanocinnamic (**39** and **51**) moiety were very similar, their different activity was quite surprising. On this basis, because the analysis of the binding mode of such compounds within NNBP does not allow for the full rationalization of biological data, and additional simulations are required to account for either the flexibility of NNBP or the events leading to the opening of the allosteric pocket and to the penetration of inhibitors into NNBP.

Computational Studies on the K103N Mutant. The crystal structure of the K103N apoenzyme (PDB entry 1HQE)³² shows a hydrogen bond between side chains of Asn103 and Tyr188

(an analogous hydrogen bond contact does not exist in the wt RT structure) and additional interactions with two neighboring water molecules. Because this hydrogen bond network was suggested to stabilize the closed-pocket form of the mutant enzyme in the unligated state, it was reasonable to hypothesize that it could interfere with NNRTIs entry. Consequently, it has been proposed that the K103N substitution is the key structural element responsible for a novel mechanism of drug resistance, based on the stabilization of the closed form of NNBP. In addition, crystallographic complexes between several inhibitors and wt or K103N RT revealed comparable binding modes and similar enzyme–inhibitor interactions.³³ In a similar way, calculations performed by us to dock the new inhibitors on both wt and K103N RT found comparable binding modes into the NNBP (without any interaction with the mutated residue) that did not allow for the rationalization of different activities toward RT.

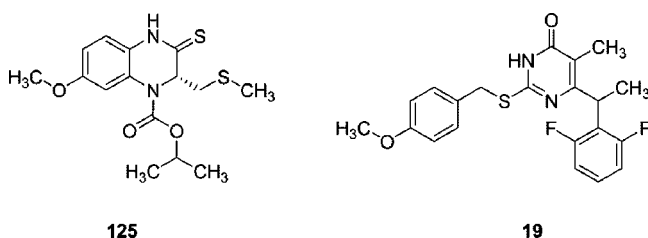
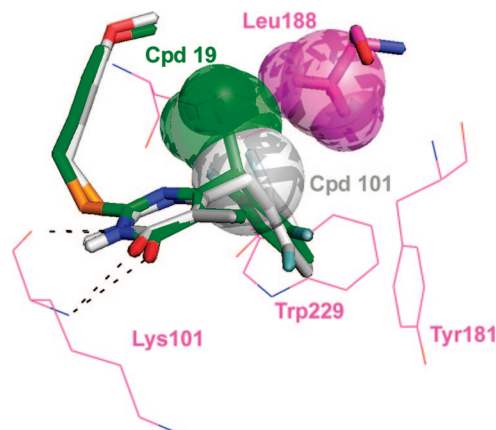
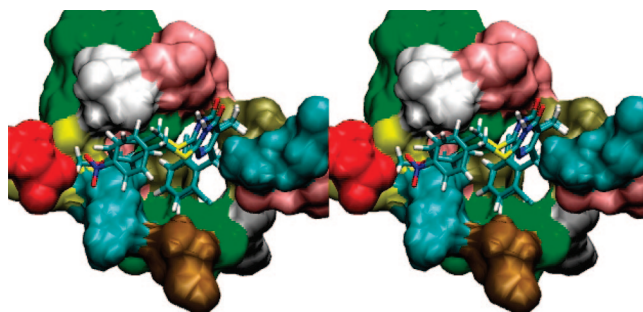
With the aim to better clarify the resistance profile of the inhibitors toward mutant K103N RT, the behavior of *S*-DABO derivatives and efavirenz was investigated at the entrance of the binding pocket of a closed form of the mutant enzyme (crystal structure PDB code 1HQE)³⁰ by MD simulations in explicit solvent. The full results of these studies will be subject matter of a dedicated publication that is in preparation at the moment. In this paper, we anticipate the results of the MD studies carried on the *R*-enantiomers of derivatives **21** and **49** (both synthesized as racemates and endowed with similarly strong inhibitory activity toward K103N RT), selected as model structures of the whole set. These results are compared here, with those obtained on two previously synthesized derivatives, **94** and **96**, which, differently, showed similar strong inhibitory potency toward wt RT, coupled with a completely different potency toward the K103N mutation (only **96** has been found to be significantly active).²¹ We have in fact evaluated the SAR characteristics of **94** and **96** to be optimum for the identification of a model, at a molecular level, of the resistance profile of our *S*-DABO derivatives. Notably, the structures of **94** and **96**, less-functionalized than those of **21** and **49**, are very similar to each other, differing only for the *para*-substituent at the benzylthio side chain: OCH₃ in the case of **94** and NO₂ in the case of **96**.

AutoDock software was used to place compounds **94** and **96** at the entrance of the NNBP of 1HQE. The structures of the two inhibitors docked at the entrance of NNBP are shown in Figure 5. The most populated cluster provided a reasonable entry

Table 10. QSAR Results: Details on Actual and Estimated/Predicted Activity Values

training set	pEC ₅₀			test set	pEC ₅₀		
	exp.	pred.	Δ		exp.	pred.	Δ
100	3.87	4.28	-0.41	118	3.87	5.25	-1.38
32	3.87	5.37	-1.50	38	3.87	6.25	-2.38
111	3.87	6.47	-2.60	34	3.87	5.22	-1.35
37	3.87	5.56	-1.69	115	3.87	3.19	0.68
105	3.87	5.08	-1.21	33	3.87	5.70	-1.83
27	3.87	3.29	0.58	54	4.40	5.53	-1.13
28	3.87	3.43	0.44	35	4.79	6.51	-1.72
112	4.47	4.95	-0.48	121	4.89	-6.94	11.83
88	4.58	5.87	-1.29	93	5.60	4.91	0.69
14	4.64	3.42	1.22	52	5.61	5.80	-0.19
25	4.69	4.39	0.30	39	5.76	6.59	-0.83
110	4.75	5.83	-1.08	117	5.88	7.28	-1.40
59	5.41	8.65	-3.24	57	5.92	7.29	-1.37
87	5.47	5.79	-0.32	106	6.10	5.44	0.66
86	5.57	5.86	-0.29	92	6.17	6.75	-0.58
89	5.74	6.13	-0.39	43	6.32	6.80	-0.48
103	6.05	5.82	0.23	114	6.33	5.33	1.00
95	6.08	7.08	-1.00	11	6.43	6.92	-0.49
96	6.10	6.75	-0.65	12	6.70	8.90	-2.20
41	6.21	6.38	-0.17	116	6.77	5.82	0.95
51	6.23	8.02	-1.79	48	6.85	7.93	-1.08
113	6.24	7.36	-1.12	46	6.85	7.71	-0.86
53	6.30	7.07	-0.77	91	7.00	5.28	1.72
30	6.43	6.41	0.02	90	7.06	7.00	0.06
98	6.51	6.06	0.45	3	7.36	6.67	0.69
44	6.59	6.44	0.15	45	7.37	7.60	-0.23
108	6.60	6.04	0.56	55	7.68	6.41	1.27
107	6.70	8.01	-1.31	42	8.05	7.99	0.06
7	6.80	7.12	-0.32	20	8.11	8.03	0.08
99	6.82	6.46	0.36	23	8.31	8.39	-0.08
13	6.82	6.47	0.35	22	8.72	6.91	1.81
120	6.93	5.59	1.34	8	8.89	8.35	0.54
97	6.96	5.71	1.25	5	8.96	8.09	0.87
102	7.13	6.54	0.59	119	9.36	7.48	1.88
18	7.13	7.39	-0.26	49	9.70	8.99	0.71
4	7.18	6.50	0.68	24	9.70	9.24	0.46
56	7.20	7.66	-0.46	9	9.70	8.79	0.91
104	7.28	6.70	0.58	1	6.89	7.20	-0.31
101	7.59	7.67	-0.08	15	6.85	8.01	-1.16
6	7.72	6.93	0.79	17	7.12	7.56	-0.44
36	7.82	6.72	1.10	26	5.34	3.77	1.57
16	7.92	8.53	-0.61	31	5.42	5.96	-0.54
94	8.17	6.79	1.38	29	5.97	6.42	-0.45
21	8.48	7.84	0.64				
2	8.66	7.64	1.02				
40	8.82	7.55	1.27				
58	8.96	8.57	0.39				
50	9.40	7.78	1.62				
10	9.70	8.75	0.95				
47	9.70	8.90	0.80				
109	9.85	7.51	2.34				
19	10.60	9.00	1.60				

point, common to both compounds, showing the 2,6-dichlorobenzyl substituent at position 6 of the pyrimidinone ring accommodated in a hydrophobic pocket mainly defined by Gly99, Lys101, Ile135, Tyr181, Tyr319, Pro321, and Trp383

**Figure 3.** Chemical structure of the quinoxaline derivative **125** and the S-DABO **19**.**Figure 4.** Binding mode of **19** (*R*-enantiomer) and **101** into NNBP of Y188L mutant.**Figure 5.** Stereoview (wall-eyed) of the superposition of **94** and **96**, docked at the entrance of the NNBP of 1HQE. Only the surface of the enzyme corresponding to residues playing a leading role is shown according to the following color codes: Asn (yellow), Asp (red), Glu (pink), Gly (tan), Ile (tan), Leu (pink), Lys (cyan), Pro (ochre), Trp (silver), Tyr (green), and Val (white). On the right side, POCKET 1 is occupied by the 2,6-dichlorobenzyl substituent at position 6 of the pyrimidinone ring. On the left, Asn103 (yellow) and Asp192 (red) contour the *para*-substituent on the benzylthio side chain. Val179 appears in white color on the upper left of the figure between Tyr188 and Tyr181 (green).

(POCKET 1). The pyrimidinone ring was located in close proximity of a prevalently polar small crevice, formed by residues Glu28, Lys32, and Glu138, while both the benzylthio side chains at position 2 pointed the *para*-substituent (*p*-methoxy and *p*-nitro) toward Lys101, Asn103, and Asp192. Remarkably, this location at the interface between the two subunits fits the binding site proposed for nevirapine, efavirenz, and etravirine.³⁰

Supramolecular assemblies were then built adding TIP3P water molecules to each complex, as found by AutoDock, which were subjected to a MD procedure ending with the geometry optimization of the output (see the Experimental Section). Comparison among minimized enzyme–inhibitor complexes filtered by MD was selected as the rule to make SAR considerations. MD filtering, in fact, supplied each complex with a peculiar mutual induced fit derived by the interactions between the inhibitor and the enzyme, a sort of “dynamic memory” that helped to interpret the very first moments of a possible opening of RT NNBP.

The complexes between K103N RT and, respectively, **94**, **96**, *R*-**21**, and *R*-**49** are shown in sequence in Figure 6. In the case of **94** and **96**, the 2,6-dichlorobenzyl substituents at position 6 of both compounds resulted to be almost superimposable, still accommodated into POCKET1. The pyrimidinone rings as well, both still located in proximity of residues Glu28, Lys32, and Glu138, with the NH and CO groups directed toward the solvent,

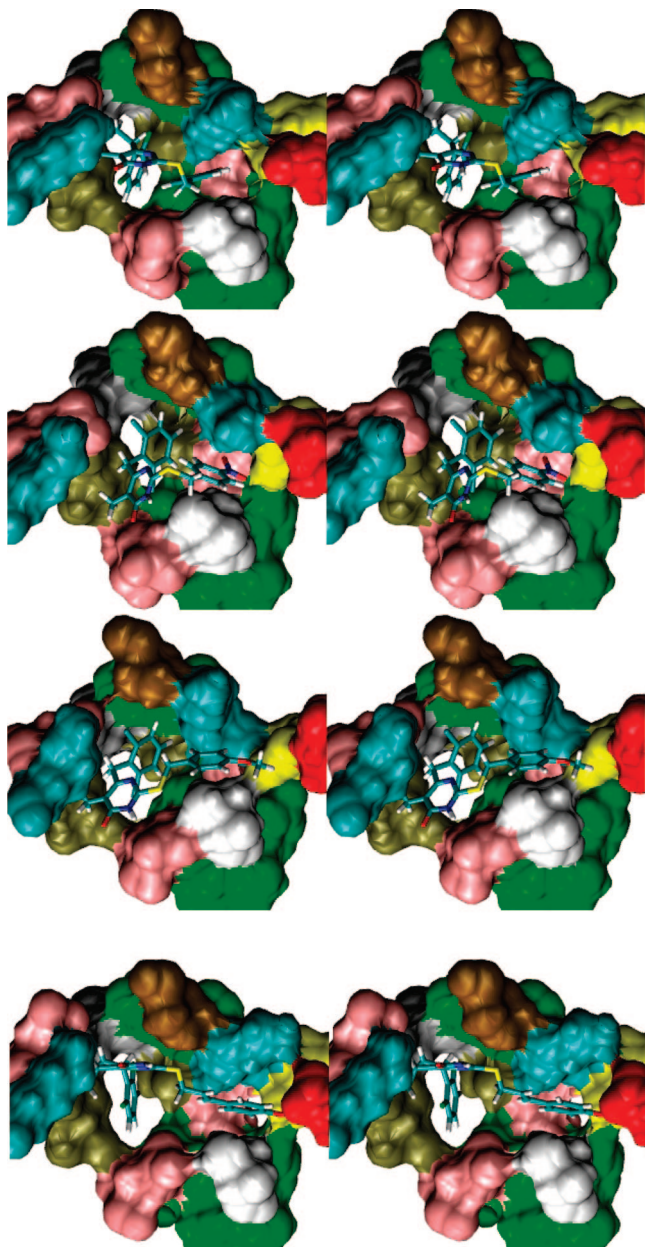


Figure 6. Stereoview (top-down) of the MD filtered enzyme-inhibitor complexes of, respectively, **94**, **96**, *R-21* and *R-49*. Only the surface of the enzyme corresponding to residues playing a leading role is shown. Color codes are described in the captions of Figure 5, as well as the location of crucial residues. Notably, in the case of **96**, *R-21*, and *R-49* complexes, the pink surface of Leu100 (located within the NNBP of RT) appears in large on the left of the figure, between Tyr188 and Tyr181 (green) and below Val179 (white), testifying the beginning of the formation of the binding pocket.

were partially superimposable to each other, while the benzylthio side chains at position 2, differently substituted in **94** and **96**, were accommodated in different areas at the NNBP entrance. In the case of **94**, the benzylthio chain retained the interaction pattern detected by the preliminary docking, being still outward, directed to residues Lys101, Asn103, and Asp192. In the case of **96**, conversely, the side chains of residues Lys101 and Val179 shaped a sort of crevice that accommodated the benzylthio moiety. In this orientation, the *p*-nitro substituent was able to form a hydrogen bond with Asn103. Due to this interaction, this residue disrupted the H-bond with Tyr188, which has been reported as one of the major hurdles hampering the creation of the NNBP.³⁰ Notably, because of the interaction with Asn103,

the sole benzylthio chain of **96** was able to penetrate in the entrance of the NNBP, beginning to push residues Val179 and Tyr181 away from Tyr188.³¹

The orientation of *R-21* at the NNBP entrance was strongly reminiscent of that of compound **96** (Figure 6), and the structures of both compounds are very similar to each other. In particular, the benzylthio chain of the former compound gave the pattern of intermolecular interactions already described in the case of the latter one. Therefore, the activity of derivative **21** could be related as well to the ability of this compound to disrupt the H-bond between Asn103 and Tyr188, probably due to the presence of a *p*-nitro substituent.

Differently from compound **94**, derivative **49** still keeps a valuable inhibitory activity toward K103N RT (both compounds share the *p*-methoxy substituent). Our MD studies on the NNBP entrance helped to rationalize the potency of the latter derivative toward K103N RT as due to its peculiar interaction pattern with the unliganded enzyme. The 2,6-difluorobenzyl substituent of *R-49*, in fact, resulted to be still accommodated into POCKET 1, while the pyrimidinone ring was slightly shifted with respect to the case of the corresponding moiety of **96** and *R-21*, toward residues Lys32 and Pro321. Due to this peculiar orientation, the rigid cynamylthio moiety, replacing the benzylthio chain of **96** and *R-21*, was able to interact by H-bond with Asn103 and to disrupt the interaction of this residue with Tyr188. In this way, this chain was able to penetrate in the entrance of the NNBP, beginning to push residues Val179 and Tyr181 away from Tyr188.

In conclusion and differently from docking, MD simulations detected differences in the interaction pattern of the studied inhibitors at the NNBP entrance, which allowed to foresee their different inhibitory potencies toward K103N RT, depending on their different capabilities to open the non-nucleoside binding pocket.

Conclusions

In the context of our ongoing effort in the preparation of novel potent NNRTIs, a number of highly functionalized *S*-DABO derivatives were prepared by means of parallel synthesis and with the aid of microwave-assisted organic chemistry. Results from both anti-HIV RT assays and HIV activity in lymphoid cells highlighted, for the majority of compounds, high potency and low cytotoxicity. In particular, compound **19** showed an anti-HIV-1 profile undoubtedly superior to that of nevirapine and comparable to that of efavirenz, thus emerging as the most active RT inhibitor (wt enzyme) reported so far. Nevertheless, biological data obtained on relevant mutants were less encouraging and led us to carry out a deeper analysis by means of computational chemistry techniques. The docking protocol, successfully applied to rationalize the relationships between the molecular structure of the inhibitors and their activity toward wt RT, Y188L, and Y181C failed in the case of K103N mutation. However, for this particular mutant, the application of a molecular dynamics protocol allowed the rationalization of the biological data on the basis of the different capability of selected compounds to open the NNBP and to interact with fundamental aminoacidic residues.

Starting from our molecular scaffold, it is our firm intention for the future to take advantage of all this knowledge to design and synthesize selected compounds able to inhibit not only the

wt virus but also the most common and clinically relevant mutant strains of the virus itself.

Experimental Section

Chemistry. Reagents were obtained from commercial suppliers and used without further purifications. According to standard procedures, CH_2Cl_2 was dried over calcium hydride, MeOH and EtOH were dried over Mg/L_2 , THF was dried over Na/benzophenone prior to use, and DMF was bought already anhydrous. Anhydrous reactions were run under a positive pressure of dry N_2 or argon. IR spectra were recorded on a Perkin-Elmer BX FT-IR system using CHCl_3 as the solvent. TLC was carried out using Merck TLC plates, Kieselgel 60 F₂₅₄. Chromatographic purifications were performed on columns packed with Merck 60 silica gel, 23–400 mesh, for flash technique. Melting points were taken using a Gallenkamp melting point apparatus and are uncorrected. ^1H NMR spectra were recorded with a Bruker AC200F spectrometer at 200 MHz, and chemical shifts are reported in δ values, relative to TMS at δ 0.00 ppm. CD_3OD , $\text{DMSO}-d_6$, and CD_3Cl were used as solvents. Buchi Syncore polyvap was used for parallel synthesis, filtration, and evaporation.

HPLC and MS Analysis. The purity of the compounds was assessed by reversed-phase liquid chromatography and mass spectrometry (Agilent series 1100 LC/MSD) with a UV detector at $\lambda = 254$ nm and an electrospray ionization source (ESI). The LC elution method (using Hypersil ODS, 4.6 mm \times 200 mm, 5 μm C18 column; Zorbax Eclipse XDB, 4.6 mm \times 150 mm, 5 μm C8 column) was the following: 20 min method at 25 °C, mobile phase composed of different MeOH/ H_2O or $\text{CH}_3\text{CN}/\text{H}_2\text{O}$ mixtures at a flow rate of 1 mL/min (all solvents were HPLC grade, Fluka). Mass spectral (MS) data were obtained using an Agilent 1100 LC/MSD VL system (G1946C) with a 0.4 mL/min flow rate using a binary solvent system of 95:5 MeOH/water. UV detection was monitored at 254 nm. Mass spectra were acquired in positive mode, scanning over the mass range of 50–1500. The following ion source parameters were used: drying gas flow, 9 mL/min; nebulizer pressure, 40 psig; drying gas temperature, 350 °C.

Microwave Irradiation Experiments. Microwave reactions were conducted using a CEM Discover Synthesis Unit (CEM Corp., Matthews, NC). The machine consists of a continuous focused microwave-power delivery system with operator-selectable power output from 0 to 300 W. The temperature of the contents of the vessel was monitored using a calibrated infrared temperature control mounted under the reaction vessel. All experiments were performed using a stirring option, whereby the contents of the vessel are stirred by means of a rotating magnetic plate located below the floor of the microwave cavity and a Teflon-coated magnetic stir bar in the vessel.

Synthesis. Parallel Synthesis of Substituted Phenylacetic Acids 71–74. A 2.0 M solution of LDA in heptane/THF/ethylbenzene (8.83 mL, 17.43 mmol) was placed in three different vessels of the Buchi Syncore and cooled (0 °C). Appropriate phenylacetic acids (5.81 mmol) were added portionwise to these solutions, and then HMPA (1.52 mL, 8.71 mmol) and THF (4 mL) were added to the mixtures. The resulting solutions were stirred (270 rpm) at room temperature for 30 min and then they were recooled (0 °C), treated with appropriate alkyl iodide (8.71 mmol), and stirred (270 rpm) at room temperature for 1 h. After being stirred, water (10 mL) and 2 N HCl (7 mL) were added to the cooled solutions, and the resulting mixtures were stirred (270 rpm) for an additional 10 min. The products were extracted in parallel with ethyl acetate (3 \times 10 mL). The organic phases, separated with a specific filtration unit, were combined and evaporated to dryness with the same apparatus to give 71–74 as pure compounds. Spectroscopic and analytical data for compounds 71–74 are in agreement with those reported in the literature.^{32,33}

Parallel Synthesis of β -Keto Esters 77–85. General Procedure. Potassium ethyl 2-methylmalonate (0.929 g, 5.04 mmol) and potassium ethyl 2-ethylmalonate (0.999 g, 5.04 mmol) were placed in six and three different vessels of the Buchi Syncore, respectively. These compounds were suspended in dry acetonitrile

(6 mL). Triethylamine (1.07 mL, 7.67 mmol) and magnesium chloride (0.571 g, 6 mmol) were added to the stirred suspensions and the mixtures were stirred (360 rpm) at room temperature for 2 h and then were added the solutions of (substituted phenylacetyl) imidazolides in dry acetonitrile, prepared 15 min before by a reaction between appropriate phenylacetic acid (2.4 mmol) and *N,N'*-carbonyldiimidazole (0.427 g, 2.67 mmol) in acetonitrile (3 mL). The reaction mixtures were stirred (360 rpm) overnight at room temperature and then refluxed for 2 h. A total of 6 mL of 13% HCl was added dropwise to the cooled mixtures, and the resulting clear mixtures were stirred (360 rpm) for an additional 10 min. Finally, the organic layers were separated in parallel with a specific filtration unit. The aqueous phases were extracted once with ethyl acetate (10 mL), and the organic phases were combined and then evaporated to dryness in parallel with the same apparatus to give 77–85 as oils to be used in the next step without further purification. Spectroscopic and analytical data for compounds 77 and 80–82 are in agreement with those reported in the literature.^{18,32,34,35}

Parallel Synthesis of Thiouracils (60–68). General Procedure. Sodium (0.105 g, 4.55 mmol) was placed in nine different vessels of the Buchi Syncore and dissolved in 8 mL of anhydrous ethanol under a positive pressure of dry N_2 . Thiourea (0.241 g, 3.178 mmol) and 77–85 (2.27 mmol) were added in different vessels, and the resulting mixtures were shaken overnight at reflux temperature at 360 rpm. Then, solvent was evaporated in parallel, and the residues were redissolved in the least amount of water (3 mL). After neutralization with 0.5 N acetic acid, the products were extracted in parallel with ethyl acetate (3 \times 10 mL). The organic phases, separated with a specific filtration unit, were combined and evaporated to dryness with the same apparatus. Finally, the residues were washed twice with petroleum ether to give compounds 60–68, pure enough to be used in the next step without purification. Spectroscopic and analytical data for compounds 61–65 are in agreement with those reported in the literature.^{32,34,35}

Method A. General Procedure Microwave-Assisted Synthesis of Substituted 6-Benzyl-2-(benzylthio)-5-alkylpyrimidin-4(3H)-ones 1–7, 11, 12, 14–22, and 25–28. Compounds 60–65 and 66–88 (0.3 mmol) and the appropriate halobenzyl derivatives (0.3 mmol) were suspended in the least amount of dry DMF (0.7 mL) in sealed vessels in the presence (60–62) or not (63–65, 67, 68) of K_2CO_3 (0.041 g, 0.3 mmol), and the mixtures were irradiated at 130 °C for 5 min. The reaction mixtures were then diluted with water (2 mL) and extracted with ethyl acetate (3 \times 10 mL). Finally, the organic phases were dried over anhydrous Na_2SO_4 and evaporated to dryness. The residues were purified by crystallization to give compounds 1–7, 11, 12, 14–22, and 25–28 in very high purity. Compound 22 was obtained pure after purification on silica gel.

Method A. Examples. 4-(4-(2,6-Dichlorobenzyl)-5-methyl-6-oxo-1,6-dihydro-pyrimidin-2-ylmethylthio)-benzoic Acid Methyl Ester (1). Yield 67%. Mp 212–216 °C. IR (CHCl_3 , ν , cm^{-1}): 1291, 1721, 3017. ^1H NMR ($\text{DMSO}-d_6$): δ 2.04 (s, 3H), 3.81 (s, 3H), 4.07 (s, 2H), 4.19 (s, 2H), 6.96 (d, 2H, $J = 8.4$), 7.23 (t, 1H, $J = 7.3$), 7.43 (d, 2H, $J = 7.3$), 7.71 (d, 2H, $J = 8.4$). MS (ESI) m/z : 449 $[\text{M} + \text{H}]^+$, 471 $[\text{M} + \text{Na}]^+$. HPLC (C_8 column; $\text{CH}_3\text{OH}/\text{H}_2\text{O}$, 75/25) t_R 7.32 min. Anal. ($\text{C}_{21}\text{H}_{18}\text{F}_2\text{N}_2\text{O}_5\text{S}$) C, H, S, N.

6-(1-(2,6-Dichlorophenyl)-ethyl)-2-(4-methoxybenzylthio)-5-methylpyrimidin-4(3H)-one (5). Yield 67%. Mp 188–190 °C. IR (CHCl_3 , ν , cm^{-1}): 1513, 1641, 3008. ^1H NMR (CDCl_3): δ 1.60 (s, 3H), 1.65 (d, 3H, $J = 7.1$ Hz), 3.77 (s, 3H), 4.38 (d, 1H, $J = 13.6$ Hz), 4.51 (d, 1H, $J = 13.6$ Hz), 4.89 (q, 1H, $J = 7.1$ Hz), 6.79–7.31 (m, 7H). MS (ESI) m/z : 435 $[\text{M} + \text{H}]^+$, 457 $[\text{M} + \text{Na}]^+$. HPLC (C_8 column; $\text{CH}_3\text{OH}/\text{H}_2\text{O}$, 80/20) t_R 7.17 min. Anal. ($\text{C}_{21}\text{H}_{20}\text{Cl}_2\text{N}_2\text{O}_2\text{S}$) C, H, S, N.

Method B. General Procedure for the Preparation of Compounds 29–32, 55–59. Appropriate thiouracil (0.3 mmol) and 1-(2-bromoethoxymethyl)-4-methoxybenzene (0.3 mmol) or the appropriate phenacyl bromide (0.4 mmol) were suspended in the least amount of dry DMF in the presence of K_2CO_3 (0.3 mmol), and the mixture was stirred at room temperature for 2 h. The reaction mixture was then diluted with water (2 mL) and extracted with

ethyl acetate (3 × 10 mL). Finally, the organic phases were dried over anhydrous Na₂SO₄ and evaporated to dryness. The residues were purified by crystallization to give compounds **29–32** and **55–59** in very high purity.

Method B. Examples. 6-(2,6-Dichlorobenzyl)-2-(4-cyanophenylthio)-5-methylpyrimidin-4(3H)-one (29). Yield 42%. Mp 256 °C (dec). IR (Nujol, ν , cm⁻¹): 2951, 2225, 1691, 1633. ¹H NMR [(CD₃)₂SO]: δ 1.99 (s, 3H), 4.03 (s, 2H), 4.43 (s, 2H), 6.95–7.03 (m, 3H), 7.87 (d, 2H, J = 8.1 Hz), 8.04 (d, 2H, J = 8.1 Hz), 12.71 (bs, 1H). MS (ESI) m/z : 444 [M + 1], 466 [M + Na]. Anal. (C₂₀H₁₃Cl₂N₃O₂S) C, H, S, N.

6-(1-(2,6-Difluorophenyl)-ethyl)-2-(2-(4-methoxybenzyloxy)ethylsulfanyl)-5-ethylpyrimidin-4(3H)-one (59). Yield 34%. Mp 143–145 °C. IR (CHCl₃, ν , cm⁻¹): 1645, 2934. ¹H NMR (CDCl₃): δ 0.98 (t, 3H, J = 7.2 Hz), 1.62 (d, 3H, J = 6.8 Hz), 2.50 (q, 2H, J = 7.2 Hz), 3.29–3.34 (m, 2H), 3.54–3.61 (m, 2H), 3.78 (s, 3H), 4.42 (s, 2H), 4.58 (q, 1H, J = 6.8 Hz), 6.79–6.86 (m, 4H), 7.12–7.29 (m, 3H). MS (ESI) m/z : 461 [M + H]⁺, 483 [M + Na]⁺. HPLC (C₈ column; CH₃OH/H₂O, 80/20) t_R 5.21 min. Anal. (C₂₄H₂₆F₂N₂O₃S) C, H, S, N.

Method C. General Procedure. Microwave-Assisted Synthesis of Substituted 6-Benzyl-2-(benzylthio)-5-alkylpyrimidin-4(3H)-ones 10, 13, 23, 39, 41, 43, 45–51, 54. Appropriate benzyl alcohol derivatives (0.3 mmol) were suspended in the least amount of dry DMF (1 mL) in the presence of trimethylphosphine (0.45 mL, 1 M solution in toluene) and swollen for 10 min. The reaction mixtures were cooled in ice bath, and CBr₄ (0.15 g, 0.45 mmol) was added. The mixtures were irradiated at 40 °C for 5 min, and then compounds **61–63**, **65**, and **66** (0.3 mmol) were added. The reaction mixtures were irradiated at 130 °C for 5 min and then were diluted with water (2 mL) and extracted with diethyl ether (5 × 10 mL). Finally, the combined organic phases were dried over anhydrous Na₂SO₄ and evaporated to dryness. The residues were purified on silica gel by flash chromatography and recrystallized by using a suitable solvent to give compounds **10**, **13**, **23**, **39**, **41**, **43**, **45–51**, and **54** in very high purity.

Method C. Examples. 6-(1-(2,6-Dichlorophenyl)-ethyl)-2-(2-(4-methoxyphenyl)propylthio)-5-methylpyrimidin-4(3H)-one (10). Yield 64%. Mp 164–166 °C. IR (CHCl₃, ν , cm⁻¹): 1536, 1651, 2937. ¹H NMR (CD₃OD): 1.53 (s, 3H), 1.57 (d, 3H, J = 7.2 Hz), 1.98–2.05 (m, 2H), 2.67 (t, 2H, J = 7.2 Hz) 3.06–3.29 (m, 2H), 3.72 (s, 3H), 4.92 (q, 1H, J = 7.1 Hz), 6.79 (d, 2H, J = 8.7 Hz), 7.05–7.21 (m, 3H), 7.33 (d, 2H, J = 8.6 Hz). MS (ESI) m/z : 463 [M + H]⁺, 485 [M + Na]⁺. HPLC (C₈ column; CH₃OH/H₂O, 80/20) t_R 12.93 min. Anal. (C₂₃H₂₄Cl₂N₂O₂S) C, H, S, N.

6-(2,6-Difluorobenzyl)-2-(3-(4-nitrophenyl)propynylsulfanyl)-5-methylpyrimidin-4(3H)-one (54). Yield 67%. Mp 223–225 °C. IR (CHCl₃, ν , cm⁻¹): 1643, 2931, 3368. ¹H NMR (DMSO-*d*₆): δ 2.02 (s, 3H), 3.93 (s, 4H), 6.95–6.99 (m, 1H), 7.15–7.35 (m, 2H), 7.51 (d, 2H, J = 8.5 Hz), 8.18 (d, 2H, J = 8.5 Hz). MS (ESI) m/z : 428 [M + H]⁺. HPLC (C₈ column; CH₃OH/H₂O, 80/20) t_R 4.10 min. Anal. (C₂₁H₁₅F₂N₃O₃S) C, H, S, N.

Method D. General Procedure. Microwave-Assisted Synthesis of Substituted 6-Benzyl-2-(benzylthio)-5-alkylpyrimidin-4(3H)-ones 8, 9, 24, 36–38, 40, 42, 44, 52, 53. Compounds **60–64** (0.3 mmol) and appropriate benzyl alcohol derivatives (0.3 mmol) were suspended in the least amount of dry DMF (1 mL) in the presence of trimethylphosphine (0.3 mL, 1 M solution in toluene). The reaction mixtures were cooled in ice bath, and DIAD was added (0.3 mmol). The mixtures were irradiated at 40 °C for 10 min and then were diluted with water (2 mL) and extracted with diethyl ether (5 × 10 mL). Finally, the combined organic phases were dried over anhydrous Na₂SO₄ and evaporated to dryness. The residues were purified on silica gel by flash chromatography and recrystallized by using a suitable solvent to give compounds **8**, **9**, **24**, **36–38**, **40**, **42**, **44**, **52**, and **53** in very high purity.

Method D. Examples. 6-(2,6-Difluorobenzyl)-2-(2-(4-methoxyphenyl)ethylthio)-5-ethylpyrimidin-4(3H)-one (24). Yield 65%. Mp 173–174 °C. IR (CHCl₃, ν , cm⁻¹): 1535, 1662, 2964. ¹H NMR (DMSO-*d*₆): δ 1.14 (t, 3H, J = 7.5 Hz), 2.63 (q, 2H, J = 7.5 Hz), 2.65 (t, 2H, J = 7.3 Hz), 2.91 (t, 2H, J = 7.3 Hz), 3.66 (s, 3H),

3.98 (s, 2H), 6.72–7.23 (m, 7H). MS (ESI) m/z : 417 [M + H]⁺, 439 [M + Na]⁺. HPLC (C₈ column; CH₃OH/H₂O, 80/20) t_R 4.20 min. Anal. (C₂₂H₂₂F₂N₂O₂S) C, H, S, N.

6-(2,6-Dichlorobenzyl)-2-(3-(4-methoxyphenyl)-allylsulfanyl)-5-methylpyrimidin-4(3H)-one (36). Yield 75%. Mp 211–212 °C. IR (CHCl₃, ν , cm⁻¹): 1539, 1660, 3002. ¹H NMR (DMSO-*d*₆): δ 2.03 (s, 3H), 3.47 (d, 2H, J = 7.2 Hz), 3.72 (s, 3H), 4.18 (s, 2H), 5.62–5.73 (m, 1H, J = 7.2 Hz, J_{trans} = 15.5 Hz), 6.24 (d, 1H, J_{trans} = 15.5 Hz), 6.85–6.89 (m, 2H), 7.13–7.44 (m, 5H). MS (ESI) m/z : 447 [M + H]⁺, 469 [M + Na]⁺. HPLC (C₈ column; CH₃OH/H₂O, 80/20) t_R 6.34 min. Anal. (C₂₂H₂₀Cl₂N₂O₂S) C, H, S, N.

Method E. General Procedure for the Preparation of Compounds 33–35. Thiouracil (**60** or **62**, 0.60 mmol), and 4-substituted-cyanoamoylboronic acid (1.80 mmol), Cu(OAc)₂ (0.60 mmol), and 1,10-phenanthroline (1.20 mmol) were mixed in dry 1,2-DCE (3 mL) in the presence of molecular sieves (2.00 g) under N₂. The reaction mixture was irradiated at 85 °C for 10 min, then cooled down and filtered on silica gel. The organic solvent was evaporated at reduced pressure to give a crude product that was recrystallized from a suitable solvent.

Method E. Examples. 6-(2,6-Dichlorobenzyl)-2-(2-(4-fluorophenyl)-vinylsulfanyl)-5-methylpyrimidin-4(3H)-one (33). Yield 35%. Mp 267–268 °C. IR (Nujol) (ν , cm⁻¹): 2942, 1643. ¹H NMR (DMSO-*d*₆): δ 2.06 (s, 3H), 4.19 (s, 2H), 6.70 (d, 1H, J = 16.4 Hz), 6.92 (d, 1H, J = 16.4 Hz), 7.14–7.47 (m, 7H), 12.67 (bs, 1H). MS (ESI) m/z : 421 [M + H]⁺, 443 [M + Na]⁺, 459 [M + K]⁺. Anal. (C₂₀H₁₅Cl₂FN₂O₂S) C, H, S, N.

6-(2,6-Dichlorobenzyl)-2-(2-(4-methoxyphenyl)-vinylsulfanyl)-5-methylpyrimidin-4(3H)-one (34). Yield 50%. Mp 199–201 °C. IR (CHCl₃, ν , cm⁻¹): 1527, 1632, 2945. ¹H NMR (DMSO-*d*₆): δ 2.06 (s, 3H), 3.78 (s, 3H), 4.19 (s, 2H), 6.56–6.82 (m, 3H), 6.93–7.13 (m, 4H), 7.27–7.49 (m, 2H). MS (ESI) m/z : 433 [M + H]⁺, 455 [M + Na]⁺. HPLC (C₈ column; CH₃OH/H₂O, 80/20) t_R 5.80 min. Anal. (C₂₁H₁₈Cl₂N₂O₂S) C, H, S, N.

Computational Details. QSAR Studies. Graphic manipulations and QSAR calculations were performed using Macromodel (version 8.5)³⁶ implemented in Maestro (version 7.5)³⁷ and Cerius2²⁴ (version 4.11) software, respectively, running on an Intel Xeon double processor machine.

The whole set of molecules (95), characterized by a central pyrimidinone core, was divided into a training set and a test set taking into account either the structural features or the activity profile of compounds. The training set was chosen following these recommendations: (i) The most- and less-active compounds were both included. Moreover, because inactive compounds were considered as a source of important information, they were also included in calculations with an activity value arbitrarily set to 50% of the activity value of the least active compound (i.e., compounds **37**, **105**, and **115**); (ii) compounds were chosen in such a way that the entire activity range was homogeneously sampled; and (iii) structural redundancy was avoided selecting compounds with different substituents or substitution patterns. Structurally similar compounds were included only if their activity differed by at least one log unit (as examples, **96** and **115**).

The input structures for molecular descriptor calculations and GFA simulations were obtained by means of a molecular docking/energy minimization protocol previously described.²¹ The conformer of each inhibitor was extracted from the complex with RT and submitted to the calculation of 2D and 3D molecular descriptors. A pretreatment was performed to discard descriptors unable to explain more than 5% of the whole variance. The GFA algorithm of Cerius2 was applied to descriptors to efficiently search the wide solution space and to identify the most suitable subsets of descriptors to build robust QSAR models. One million cross-over generations were set to let the system evolve toward a convergence threshold. The frequency of use of descriptors in the population of equations was chosen as the convergence criterion. Individuals in the population were set to 300 and the terms for each individual of the first randomly generated population was set to 5. The Reduce Equation parameter was set to 50 to favor simpler models through evolution. The equation length was kept as variable and only linear

terms were chosen, avoiding both quadratic and spline terms. The mutation probability, consisting in the addition of a new term in the equation, was left unaltered. The smoothing factor was set to 1.7, which, after a trial-and-error approach, resulted in the best compromise for obtaining low-dimensional models that maintained significant predictive power toward both the training and the test sets.

Unfortunately, preliminary GFA calculations based on a set of both 2D and 3D descriptors and using enzymatic or cellular data as the independent variable gave no statistically significant results. As a consequence, several attempts were performed to find the most appropriate set of dependent and independent variables to obtain acceptable correlations. As a result, 3D descriptors and enzymatic data were discarded, limiting GFA calculations to cellular data and 2D descriptors encoding for electronic, thermodynamic, information content, topological, and electrotopological properties, thus reducing the original set to only 38 variables.

Molecular Docking Studies. All calculations and manipulations were performed using Autodock 3.0²⁶ and MacroModel 8.5^{36/} Maestro,³⁷ OPLS_AA force field³⁸ was used for minimization procedures as implemented in the MacroModel software package.

Three-dimensional coordinates of the complexes between RT and HBY-097 (PDB entry 1BQN),²⁸ TNK-651 (PDB entry 1JLA),²⁹ and MSC-194 (PDB entry 1IKY)³⁰ were used as the input structure for docking calculations. For this aim, all cocrystallized water molecules were deleted, and all polar hydrogens were added using the appropriate tool in the builder module of Maestro. The structures of the new *S*-DABO derivatives were built using Maestro 3D-sketcher and fully minimized (Polak-Ribiere conjugate gradient, 0.01 kJ/Å·mol convergence).

For molecular docking purposes, a box of 70 × 70 × 70 points was set that comprised all residues constituting the NNRTI binding pocket. Starting structures of the selected compounds were randomly defined to obtain totally unbiased results. The GA-LS method was used with the default settings, while retrieving 250 docked conformations from each compound. Results from Autodock calculations were clustered using an rmsd tolerance of 1 Å and the lowest-energy conformer of the most populated cluster (the lowest-energy cluster in most cases) was selected as the most probable binding conformer. HIV-1 RT/ligand complexes were submitted to a full minimization of the whole structure to a 0.01 kJ/Å·mol gradient.

MD Simulations. The geometry of each inhibitor was optimized using the ab initio quantum chemistry program GAMESS³⁹ and the HF/6-31G* basis set to calculate partial atomic charges. Consequently, a set of atom-centered RHF HF/6-31G* charges was obtained for each inhibitor by application of ESP methodology⁴⁰ with ELPOT and PDC modules of GAMESS. Atom types and covalent and nonbonded parameters were assigned to inhibitors from those already present in the AMBER force field by analogy or through interpolation.⁴¹ System setup, Molecular dynamics (MD) and postdynamic analysis were performed with NAMD2 (v2.6)⁴² and VMD (v1.8.6)⁴³ software packages.

Supramolecular assemblies to be subjected to MD studies were built starting from appropriate AutoDock output complexes. Each complex was surrounded by a periodic box of TIP3P water molecules⁴⁴ that extended 7.0 Å from the protein atoms, and 10 Cl⁻ ions were added to conserve neutrality of the system. For each system, the number of water molecules was about 26700 and the initial dimensions of the rectangular periodic box were 112 × 86 × 107 Å.

The simulations were conducted using periodic boundary conditions and Particle-Mesh-Ewald (PME) method⁴⁵ with grid size of 115 × 90 × 110. The nonbonded cutoff was set to 12.0 Å, the switching distance to 10 Å and the nonbonded pair list distance to 14 Å. The r-RESPA multiple time step method⁴⁶ was employed with 1 fs for bonded, 2 fs short-range for nonbonded, and 4 fs for long-range electrostatic forces. SHAKE algorithm⁴⁷ was used to constrain all bonds involving hydrogen atoms. Molecules were simulated for a total of 600 ps in the NPT ensemble. The temperature was set to 310 K and controlled via Langevin thermostat with a dumping factor of 5 ps⁻¹. The pressure of 1 atm was controlled via isotropic Langevin piston barostat with an

oscillation period of 200 fs, a damping time scale of 100 fs, and a noise temperature of 310 K. The starting assemblies were relaxed by performing 2000 steps of conjugate gradient energy minimization to remove unfavorable contacts. The refined structures were then subjected to 200 ps of MD with harmonic restraints at minimized atomic positions of the ligand with constant of force of 1.0 Kcal mol⁻¹ Å⁻¹, followed by 200 ps of MD with constant of force of 0.5 Kcal mol⁻¹ Å⁻¹, and finally 200 ps of MD with no restraints. The final system was minimized for 1000 steps using conjugated gradient algorithm.

In Vitro Assay for Recombinant HIV-1 RT Inhibition. A 25 μL assay mixture contained 50 mM Tris-HCl, pH 7.5, 0.25 mg/ml BSA, 1 mM DTT, 10 mM MgCl₂, 10 mM [³H] dTTP (4 Ci/mmol), 0.5 μg of poly(rA)₂₀₀/oligo(dT)₂₀, 4 nM HIV-1 RT, and the inhibitor to be tested. Incorporated radioactivity was measured by quantification of acid-precipitable material on GF/C filters by liquid scintillation counting. A range of inhibitor concentrations between 0.1- and 10-fold the ID₅₀ were used. The 50% inhibitory concentration (ID₅₀) was determined by the method of Dixon.

Anti-HIV Activity in Lymphoid Cells. Biological activity of the compounds was tested in the lymphoid MT-4 cell line (received from the NIH AIDS Reagent Program) against the wt HIV-1 NL4-3 strain and three different HIV-1 strains, as described before.⁴⁸ Briefly, MT-4 cells were infected with the appropriate HIV-1 strain (or mock-infected to determine cytotoxicity) in the presence of different drug concentrations. At day five postinfection, a tetrazolium-based colorimetric method (MTT method) was used to evaluate the number of viable cells. The IRL98 HIV-1 strain contains the following mutations in the RT coding sequence: M41L, D67N, Y181C, M184V, R211K, and T215Y (conferring resistance to NRTIs) and mutations K101Q, Y181C, and G190A (conferring resistance to NNRTIs). The HIV-1 strains containing the multi-NNRTI mutation, K103N or the Y188L mutant, were received from the Medical Research Council Centralised Facility for AIDS Reagents, Herfordshire, U.K.

Time of Addition Experiments. Evaluation of the time/site of anti-HIV activity was evaluated as described before.⁴⁹ Briefly, MT-4 cells were acutely infected with wt HIV-1 NL4-3 and control or test drugs were added at different times post infection at a concentration of 100× the calculated EC₅₀. A 30 h post-infection viral p24 antigen in the supernatant is evaluated by ELISA.

Acknowledgment. This study was partially supported by grants from the European TRIOH Consortium (LSHB-2003-503480) and the Spanish MEC project BFU2006-00966 and FIS PI060624 (J.A.E.). I.C.-C. holds a FI scholarship from Generalitat de Catalunya.

Supporting Information Available: Details of synthesis and analytical data. This material is available free of charge via the Internet at <http://pubs.acs.org>.

References

- (1) Meadows, D. C.; Gervay-Hague, J. Current Developments in HIV Chemotherapy. *ChemMedChem* **2006**, *1*, 16–29.
- (2) Este, J.; Telenti, A. HIV Entry Inhibitors. *Lancet* **2007**, *370*, 81–88.
- (3) Furman, P. A.; Painter, G. R.; Anderson, K. S. An Analysis of the Catalytic Cycle of HIV-1 Reverse Transcriptase: Opportunities for Chemotherapeutic Intervention Based on Enzyme Inhibition. *Curr. Pharm. Des.* **2000**, *6*, 547–567.
- (4) Kohlstaedt, L. A.; Wang, J.; Friedman, J. M.; Rice, P. A.; Steitz, T. A. Crystal Structure at 3.5 Å Resolution of HIV-1 Reverse Transcriptase Complexed with an Inhibitor. *Science* **1992**, *256*, 1783–1790.
- (5) Jacobo-Molina, A.; Ding, J.; Nanni, R. G.; Clark, A. D., Jr; Lu, X.; Tantillo, C.; Williams, L. R.; Kamer, G.; Ferris, A. L.; Clark, P.; Hiza, A.; Hughes, S. H.; Arnold, E. Crystal Structure of Human Immunodeficiency Virus Type 1 Reverse Transcriptase Complexed with Double-Stranded DNA at 3.0 Å Resolution Shows Bent DNA. *Proc. Natl. Acad. Sci. U.S.A.* **1993**, *90*, 6320–6324.

- (6) Kati, W. M.; Johnson, K. A.; Jerva, L. F.; Anderson, K. S. Mechanism and Fidelity of HIV Reverse Transcriptase. *J. Biol. Chem.* **1992**, *267*, 25988–25997.
- (7) Menéndez-Arias, L.; Matamoros, T.; Deval, J.; Canard, B. Molecular Mechanism of Resistance to Nucleoside Analogue Inhibitors of Human Immunodeficiency Virus Reverse Transcriptase. *Drug Des. Rev.* **2005**, *2*, 101–113.
- (8) Ren, J.; Esnouf, R.; Garman, E.; Somers, D.; Ross, C.; Kirby, I.; Keeling, J.; Darby, G.; Jones, Y.; Stuart, D.; Stammers, D. High-Resolution Structures of HIV-1 RT from Four RT-Inhibitor Complexes. *Nat. Struct. Biol.* **1995**, *2*, 293–302.
- (9) Smerdon, S. J.; Jager, J.; Wang, J.; Kohlstaedt, L. A.; Chirino, A. J.; Friedman, J. M.; Rice, P. A.; Stetz, T. A. Structure of the binding site of Nonnucleoside Inhibitors of the Reverse Transcriptase of Human Immunodeficiency Virus Type 1. *Proc. Natl. Acad. Sci. U.S.A.* **1994**, *91*, 3911–3915.
- (10) De Clercq, E. Non-Nucleoside Reverse Transcriptase Inhibitors (NNRTIs): Past, Present, and Future. *Chem. Biodiversity* **2004**, *1*, 44–64.
- (11) Das, K.; Lewi, P. J.; Hughes, S. H.; Arnold, E. Crystallography and the Design of anti-AIDS Drugs: Conformational Flexibility and Positional Adaptability are Important in the Design of Non-nucleoside HIV-1 Reverse Transcriptase Inhibitors. *Prog. Biophys. Mol. Biol.* **2005**, *88*, 209–231.
- (12) Ren, J.; Stammers, D. K. HIV Reverse Transcriptase Structures: Designing New Inhibitors and Understanding Mechanisms of Drug Resistance. *Trends Pharmacol. Sci.* **2005**, *26*, 4–7.
- (13) Sarafianos, S. G.; Das, K.; Hughes, S. H.; Arnold, E. Taking Aim at Moving Target: Designing Drugs to Inhibit Drug Resistant HIV-1 Reverse Transcriptases. *Curr. Opin. Struct. Biol.* **2004**, *14*, 716–730.
- (14) Basavapathruni, A.; Anderson, K. S. Developing Novel Nucleoside HIV-1 Reverse Transcriptase Inhibitors: Beyond the Butterfly. *Curr. Pharm. Des.* **2006**, *12*, 1857–1865.
- (15) Sluis-Cremer, N.; Temiz, N. A.; Bahar, I. Conformational Changes in HIV-1 Reverse Transcriptase Induced by Nonnucleoside Reverse Transcriptase Inhibitor Binding. *Curr. HIV Res.* **2004**, *2*, 323–332.
- (16) Das, K.; Clark, A. D.; Lewi, P. J.; Heeres, J.; de Jonge, M. R.; Koymans, L. M. H.; Vinkers, K. M.; Daeyaert, F.; Ludovici, D. W.; Kukla, M. J.; De Corte, B.; Kavash, R. W.; Ho, C. Y.; Ye, H.; Lichtenstein, M. A.; Andries, K.; Pauwels, R.; de Béthune, M.-P.; Boyer, P. L.; Clark, P.; Hughes, S. H.; Janssens, P. A. J.; Arnold, E. Roles of Conformational and Positional Adaptability in Structure-Based Design of TMC125-R165335 (Etravirine) and Related Non-Nucleoside Reverse Transcriptase Inhibitors that are Highly Potent and Effective against Wild-Type and Drug-Resistant HIV-1 Variants. *J. Med. Chem.* **2004**, *47*, 2550–2560.
- (17) Botta, M.; Artico, M.; Massa, S.; Gambacorta, A.; Marongiu, M. E.; Pani, A.; La Colla, P. Synthesis, Antimicrobial and Antiviral Activities of Isotrimethoprim and Some Related Derivatives. *Eur. J. Med. Chem.* **1992**, *27*, 251–257.
- (18) Mai, A.; Artico, M.; Ragno, R.; Sbardella, G.; Massa, S.; Musiu, C.; Mura, M.; Marturana, F.; Cadeddu, A.; Maga, G.; La Colla, P. 5-Alkyl-2-alkylamino-6-(2,6-difluorophenylalkyl)-3,4-dihydropyrimidin-4(3H)-ones, a New Series of Potent, Broad-Spectrum Non-Nucleoside Reverse Transcriptase Inhibitors Belonging to the DABO Family. *Bioorg. Med. Chem.* **2005**, *13*, 2065–2077.
- (19) Ragno, R.; Mai, A.; Sbardella, G.; Artico, M.; Massa, S.; Musiu, C.; Mura, M.; Marturana, F.; Cadeddu, A.; La Colla, P. Computer-Aided Design, Synthesis, and Anti-HIV-1 Activity in Vitro of 2-Alkylamino-6-[1-(2,6-difluorophenyl)alkyl]-3,4-dihydro-5-alkylpyrimidin-4(3H)-ones as Novel Potent Non-Nucleoside Reverse Transcriptase Inhibitors, Also Active Against the Y181C Variant. *J. Med. Chem.* **2004**, *47*, 928–934.
- (20) Mugnaini, C.; Manetti, F.; Este, J. A.; Clotet-Codina, I.; Maga, G.; Cancio, R.; Botta, M.; Corelli, F. Synthesis and Biological Investigation of S-Aryl-S-DABO Derivatives as HIV-1 Inhibitors. *Bioorg. Med. Chem. Lett.* **2006**, *16*, 3541–3544.
- (21) Manetti, F.; Este, J. A.; Clotet-Codina, I.; Armand-Ugon, M.; Maga, G.; Crespan, E.; Cancio, R.; Mugnaini, C.; Bernardini, C.; Togninelli, A.; Carmi, C.; Alongi, M.; Petricci, E.; Massa, S.; Corelli, F.; Botta, M. Parallel Solution-Phase and Microwave-Assisted Synthesis of New S-DABO Derivatives Endowed with Subnanomolar Anti-HIV-1 Activity. *J. Med. Chem.* **2005**, *48*, 8000–8008.
- (22) Togninelli, A.; Carmi, C.; Petricci, E.; Mugnaini, C.; Massa, S.; Corelli, F.; Botta, M. Solution-Phase Parallel Synthesis of S-DABO Analogues. *Tetrahedron Lett.* **2006**, *47*, 65–67.
- (23) Clay, R. J.; Collom, T. A.; Karrick, G. L.; Wemple, J. A. Safe, Economical Method for the Preparation of β -Oxo Esters. *Synthesis* **1993**, *290*, 292.
- (24) *Cerius*, version 4.10; Accelrys Software, Inc.: San Diego, CA.
- (25) Kier, L. B.; Hall, L. H. *Molecular Connectivity in Chemistry and Drug Research*. Academic Press Inc., New York, 1976; p 257.
- (26) Goodsell, D. S.; Morris, G. M.; Olson, A. J. Automated Docking of Flexible Ligands: Applications of AutoDock. *J. Mol. Recognit.* **1996**, *9*, 1–5.
- (27) Hsiou, Y.; Das, K.; Ding, J.; Clark, A. D., Jr.; Kleim, J.-P.; Rösner, M.; Winkler, I.; Günter, R.; Hughes, S. H.; Arnold, E. Structures of Tyr188Leu mutant and wild-type HIV-1 reverse transcriptase complexed with the non-nucleoside inhibitor HBY 097: inhibitor flexibility is a useful design feature for reducing drug resistance. *J. Mol. Biol.* **1998**, *284*, 313–323.
- (28) Ren, J.; Nichols, C.; Bird, L.; Chamberlain, P.; Weaver, K.; Short, S.; Stuart, D. I.; Stammers, D. K. Structural mechanisms of drug resistance for mutations at codons 181 and 188 in HIV-1 reverse transcriptase and the improved resilience of second generation non-nucleoside inhibitors. *J. Mol. Biol.* **2001**, *312*, 795–805.
- (29) Lindberg, J.; Sigurdsson, S.; Lowgren, S.; Andersson, H. O.; Sahlberg, C.; Noreen, R.; Fridborg, K.; Zhang, H.; Unge, T. Structural basis for the inhibitory efficacy of efavirenz (DMP-266), MSC194 and PNU142721 towards the HIV-1 RT K103N mutant. *Eur. J. Biochem.* **2002**, *269*, 1670–1677.
- (30) Rodriguez-Barrios, F.; Balzarini, J.; Gago, F. The molecular basis of resilience to the effect of the Lys103Asn mutation in non-nucleoside HIV-1 reverse transcriptase inhibitors studied by targeted molecular dynamics simulations. *J. Am. Chem. Soc.* **2005**, *127*, 7570–7578.
- (31) Shen, L.; Shen, J.; Luo, X.; Xu, Y.; Chen, X.; Arnold, E.; Ding, J.; Jiang, H. Steered molecular dynamics simulation on the binding of NNRTI to HIV-1 RT. *Biophys. J.* **2003**, *84*, 3547–3563.
- (32) Mai, A.; Sbardella, G.; Artico, M.; Ragno, R.; Massa, S.; Novellino, E.; Greco, G.; Lavecchia, A.; Musiu, C.; La Colla, M.; Murgioni, C.; La Colla, P.; Loddio, R. Structure-based design, synthesis, and biological evaluation of conformationally restricted novel 2-alkylthio-6-[1-(2,6-difluorophenyl)alkyl]-3,4-dihydro-5-alkylpyrimidin-4(3H)-ones as non-nucleoside inhibitors of HIV-1 reverse transcriptase. *J. Med. Chem.* **2001**, *44*, 2544–2554.
- (33) Jaeger, R.; Robinson, R. Two Ketones of the Stilboestrol Group. *J. Chem. Soc.* **1941**, *131*, 744–747.
- (34) Mai, A.; Artico, M.; Sbardella, G.; Massa, S.; Novellino, E.; Greco, G.; Loi, A. G.; Tramontano, E.; Marongiu, M. E.; La Colla, P. 5-Alkyl-2-(alkylthio)-6-(2,6-dihalophenylmethyl)-3,4-dihydropyrimidin-4(3H)-ones: Novel potent and selective dihydro-alkoxy-benzyl-oxopyrimidine derivatives. *J. Med. Chem.* **1999**, *42*, 619–627.
- (35) Sbardella, G.; Mai, A.; Artico, M.; Massa, S.; Marceddu, T.; Vargiu, L.; Marongiu, M. E.; La Colla, P. Does the 2-methylthiomethyl substituent really confer high anti-HIV-1 activity to S-DABOs. *Med. Chem. Res.* **2000**, *10*, 30–39.
- (36) Mohamadi, F.; Richards, N. G. J.; Guida, W. C.; Liskamp, R.; Lipton, M.; Caufield, C.; Chang, G.; Hendrickson, T.; Still, W. C. Macro-model—an integrated software system for modeling organic and bioorganic molecules using molecular mechanics. *J. Comput. Chem.* **1990**, *11*, 440–467.
- (37) *Maestro*, version 7.5; Schrödinger: New York, 2006.
- (38) Jorgensen, W. L.; Maxwell, D. S.; Tirado-Rives, J. Development and testing of the OPLS all-atom force field on conformational energetics and properties of organic liquids. *J. Am. Chem. Soc.* **1996**, *118*, 11225–11236.
- (39) Schmidt, M. W.; Baldrige, K. K.; Boatz, J. A.; Elbert, S. T.; Gordon, M. S.; Jensen, J. H.; Koseki, S.; Matsunaga, N.; Nguyen, K. A.; Su, S.; Windus, T. L.; Dupuis, M.; Montgomery, J. A. General atomic and molecular electronic structure system. *J. Comput. Chem.* **1993**, *14*, 1347–1363.
- (40) Singh, U. C.; Kollman, P. A. An approach to computing electrostatic charges for molecules. *J. Comput. Chem.* **1984**, *5*, 129–145.
- (41) Cornell, W. D.; Cieplak, P.; Bayly, C. I.; Gould, I. R.; Merz, K. M., Jr.; Ferguson, D. M.; Spellmeyer, D. C.; Fox, T.; Caldwell, J. W.; Kollman, P. A. A second generation force field for the simulation of proteins, nucleic acids, and organic molecules. *J. Am. Chem. Soc.* **1995**, *117*, 5179–51977.
- (42) Phillips, J. C.; Braun, R.; Wang, W.; Gumbart, J.; Tajkhorshid, E.; Villa, E.; Chipot, C.; Skeel, R. D.; Kale, L.; Schulten, K. Scalable molecular dynamics with NAMD. *J. Comput. Chem.* **2005**, *26*, 1781–1802.
- (43) Humphrey, W.; Dalke, A.; Schulten, K. VMD: Visual molecular dynamics. *J. Mol. Graphics* **1996**, *14*, 33–38.
- (44) Jorgensen, W. L.; Chandrasekhar, J.; Madura, J. D.; Impey, R. W.; Klein, M. L. Comparison of simple potential functions for simulating liquid water. *J. Chem. Phys.* **1983**, *79*, 926–935.
- (45) Essman, U.; Perera, L.; Berkowitz, M. L.; Darden, T.; Lee, H.; Pedersen, L. A smooth particle mesh Ewald method. *J. Chem. Phys.* **1995**, *103* (19), 8577–8593.
- (46) Tuckerman, M.; Berne, B.; Martyna, G. Reversible multiple time scale molecular dynamics. *J. Chem. Phys.* **1992**, *97*, 1990–2001.

- (47) van Gunsteren, W. F.; Berendsen, H. J. C. Algorithms for macromolecular dynamics and constraint dynamics. *Mol. Phys.* **1977**, *34*, 1311–1327.
- (48) Armand-Ugon, M.; Gutierrez, A.; Clotet, B.; Esté, J. A. HIV-1 resistance to the gp41-dependent fusion inhibitor C-34. *Antiviral Res.* **2003**, *59*, 137–142.
- (49) Armand-Ugon, M.; Clotet-Codina, I.; Tintori, C.; Manetti, F.; Clotet, B.; Botta, M.; Esté, J. A. The anti-HIV activity of ADS-J1 targets the HIV-1 gp120. *Virology* **2005**, *343*, 141–149.

JM0708230